nature communications

Article

https://doi.org/10.1038/s41467-025-60535-5

The TRIP12 E3 ligase induces SWI/SNF component BRG1-β-catenin interaction to promote Wnt signaling

Received: 21 December 2023

Accepted: 27 May 2025

Published online: 05 June 2025

Check for updates

Sara Kassel[1,13], Kai Yuan[2,13], Nawat Bunnag[2,3], Leif R. Neitzel[4], Wenhui Lu[5], Anna Schwarzkopf[1], Benjamin Maines[2], Matthew A. Loberg[6], George Xu[6], Amber Adams[2], Andrew D. McCray[2], Alex Cho[1], Mary Rockouski[1], Gemma Orton[1], Lily Goldsmith[1], Md Mubtaseem Ahnaf Aronno[2], Zachary T. Spencer[2], Omar M. Khan[7], Fei Ye[8], Charles Williams[4], Andres M. Lebensohn[9], Rajat Rohatgi[10], Xiaofeng Wang[2,11], Vivian L. Weiss[6], Charles C. Hong[4], Arminja N. Kettenbach[3,11], David J. Robbins[5], Yashi Ahmed[2,11] ✉ & Ethan Lee[1,12] ✉

SWItch/Sucrose Non-Fermentable (SWI/SNF) chromatin remodeling complexes displace nucleosomes to promote the access of transcription factors to enhancers and promoters. Despite the critical roles of SWI/SNF in animal development and tumorigenesis, how signaling pathways recruit SWI/SNF complexes to their target genes is unclear. Here, we demonstrate that target gene activation mediated by β-catenin, the essential transcriptional coactivator in the Wnt signal transduction pathway, requires ubiquitylation of the SWI/SNF component Brahma-related gene-1 (BRG1) by the E3 ubiquitin ligase Thyroid Hormone Receptor Interactor 12 (TRIP12). TRIP12 depletion in *Drosophila*, zebrafish, mouse organoids, and human cells attenuates Wnt signaling. Genetic epistasis experiments place TRIP12 activity downstream of the β-catenin destruction complex. TRIP12 interacts with and ubiquitylates BRG1, and BRG1 depletion blocks TRIP12-mediated Wnt pathway activation. TRIP12 promotes BRG1 binding to β-catenin in the presence of Wnt. Our findings support a model in which TRIP12 ubiquitylates BRG1 in the presence of Wnt and promotes its interaction with β-catenin in the nucleus, in order to recruit SWI/SNF to Wnt target genes. Our studies suggest a general mechanism by which cell signaling induces the interaction between BRG1 and pathway-specific transcription factors to recruit SWI/SNF complexes to their appropriate target genes.

Conversion of the chromatin state of target gene promoters from an "inactive" heterochromatin into a transcriptionally "active" euchromatic conformation is a critical step in signal transduction[1]. This chromatin remodeling process is mediated by large multisubunit molecular machines termed the SWItch/Sucrose Non-Fermentable (SWI/SNF) complexes[2]. SWI/SNF complexes utilize ATP hydrolysis to slide or eject nucleosomes and facilitate the binding of transcription, replication, and repair factors to DNA[3]. Much of our understanding of SWI/SNF has focused on its composition and mechanism of chromatin remodeling. SWI/SNF complexes can bind histone modifications and

A full list of affiliations appears at the end of the paper. ✉e-mail: yashi.ahmed@dartmouth.edu; ethan.lee@vanderbilt.edu

may be guided to specific loci by recognition of the regional architecture or recruited by transcription factors. How the SWI/SNF complex is recruited to specific target genes in response to a signal, however, is not well understood.

Wnt/β-catenin signaling is an evolutionarily conserved pathway that regulates metazoan development and homeostasis[4–6]. Mutations that cause misregulation of the Wnt pathway result in developmental defects and cancer[7,8]. In the absence of Wnt ligands, the transcriptional cofactor β-catenin is phosphorylated in the cytosol by a destruction complex that maintains cytoplasmic β-catenin at low levels. Activation of the pathway results in inhibition of the destruction complex and consequent stabilization of β-catenin. β-catenin subsequently enters the nucleus and interacts with transcription factors and cofactors, including the T cell factor and lymphocyte enhancer factor (TCF/LEF) family, to promote a Wnt transcriptional program[9].

In the absence of Wnt stimulation, TCF transcription factors are normally bound to the transcriptional corepressor Groucho/Transducin-Like Enhancer (Gro/TLE), and the chromatin state of Wnt target genes is in a transcriptionally repressive form[10]. Upon pathway activation, nuclear β-catenin displaces Gro/TLE binding on TCF, and a large molecular weight nuclear complex termed the "enhanceosome"[11], consisting of the β-catenin/TCF complex and associated cofactors is proposed to assemble on and convert chromatin to a permissive form, allowing the efficient transcription of Wnt target genes[12]. Several β-catenin-associated cofactors have been identified, including B-cell lymphoma 9 (BCL9), Pygopus, p300/CREB-binding protein, and the chromatin remodeler Brahma-related gene-1/SWI/SNF-related matrix-associated actin-dependent regulator of chromatin subfamily A, member 4 (BRG1/SMARCA4 (henceforth BRG1))[13–16]. The mechanism by which these cofactors are recruited to Wnt-responsive elements in Wnt target gene promoters is not well understood.

Previous studies indicated that ubiquitylation plays an essential role in activating the β-catenin/TCF transcriptional program, particularly the transcriptional repressor Gro/TLE[17–19]. Herein, we provide biochemical, cellular, and organismal evidence that the ubiquitin ligase, Thyroid Hormone Receptor Interactor 12 (TRIP12), is an evolutionarily conserved positive regulator of Wnt signaling. We show that in the presence of Wnt, TRIP12 ubiquitylates BRG1, the catalytic component of the SWI/SNF chromatin remodeling complex, and enhances its capacity to bind β-catenin, providing a mechanism for how the SWI/SNF complex is recruited to Wnt target genes to facilitate their transcriptional activity.

Results

TRIP12 promotes Wnt/Wingless signaling in human cells, zebrafish, and *Drosophila*

We previously identified the E3 ligase TRIP12 as a positive regulator of Wnt signaling in an insertional mutagenesis screen in human HAP1 cells[20]. To confirm that TRIP12 promotes Wnt signaling in human cells, we used a human embryonic kidney (HEK) cell line that stably expresses the luciferase-based Wnt target gene reporter SuperTOPFlash (HEK293STF cells)[21]. Knockdown of TRIP12 with two independent short-interfering RNAs (siRNAs) inhibited Wnt3a-stimulated reporter activity (Fig. 1A) while having no observable effect on a constitutively active control luciferase reporter (Supplementary Fig. 1A)[22]. The inhibition of Wnt signaling by siRNA knockdown of TRIP12 was rescued with the expression of a TRIP12 siRNA-resistant construct, demonstrating the specificity of the knockdown (Supplementary Fig. 1B). Confirming the results of the Wnt reporter assay, we found that TRIP12 knockdown blocked the Wnt3a-stimulated expression of endogenous Wnt target genes, including *AXIN2*, *SP5*, and *DKK1* (Supplementary Fig. 1C). Overexpression of TRIP12 enhanced Wnt3a-mediated signaling; however, no observable activation was detected in the absence of Wnt ligand (Fig. 1B).

To assess the role of TRIP12 in regulating Wnt signaling during vertebrate development, we tested the effects of TRIP12 on Wnt signaling in zebrafish (*Danio rerio*) embryos. In zebrafish, Wnt regulates eye development, and ectopic activation of the Wnt pathway leads to an eyeless phenotype[23,24]. We found that TRIP12 overexpression gave rise to eyeless embryos, which were rescued by injecting a morpholino oligonucleotide (MO) that targets endogenous TRIP12 (Fig. 1C). The phenotypic effects of TRIP12 mRNA and MO injections were consistent with the observed changes in endogenous Wnt/β-catenin target gene expression (Fig. 1D). Disruption of Wnt/β-catenin and Wnt/planar cell polarity in zebrafish can result in malformations of the trunk axes. The formation of the dorsoventral (D-V) axis is tightly intertwined with the formation of the anteroposterior (A-P) axis, as convergent extension of the dorsolateral cells contributes to the elongation of the A-P axis. Thus, disruption of the Wnt pathway has been shown to result in trunk malformation and subsequent reduction in body length[25–27]. We found that both overexpression and CRISPRi knockdown of TRIP12 resulted in embryos with shortened axes, consistent with effects on Wnt signaling (Supplementary Fig. 2A–C). Significantly, the trunk phenotype due to TRIP12 overexpression was rescued by injection of TRIP12 MO (Supplementary Fig. 2A). We also observed that TRIP12 CRISPRi-treated embryos exhibited pericardial edema and heart malformation, consistent with previously described effects of disrupted Wnt signaling during embryogenesis[28–30] (Supplementary Fig. 2D, E). These results provide evidence that TRIP12 plays a role in Wnt signaling during early embryonic development in vertebrates.

Given the evolutionary conservation of the Wnt pathway, we evaluated the in vivo role of the *Drosophila* TRIP12 ortholog, Ctrip[31], in Wingless signaling. Mammalian TRIP12 protein has several domains: a catalytic HECT domain, two protein–protein interaction domains (Tryptophan-Tryptophan-Glutamate (WWE) and Armadillo repeats (ARM)), and an intrinsically disordered region (IDR)[32]. Alignment of the human and *Drosophila* orthologs of TRIP12 reveals a high percentage of primary sequence conservation, with 81% similarity in the ARM repeats, 46% similarity in the WWE domain, and 73% similarity in the HECT domain (Supplementary Fig. 3).

In the larval third instar wing imaginal disc, the precursor of the adult wing, Wingless is expressed in a stripe of cells at the dorsoventral boundary[33,34] and activates the transcription of the high-threshold target genes *senseless* (*sens*) and *notum*[35–37] in cells juxtaposed with the D-V boundary. Independent RNAi constructs that target different regions of *ctrip* depleted endogenous Ctrip tagged with GFP (Ctrip-GFP) efficiently (Supplementary Fig. 4). Ctrip depletion in the posterior wing disc decreased the levels of an endogenous *sens* reporter (*scarlet:sens*) in more than 45% of discs (Fig. 2D–G, Supplementary Fig. 5), in contrast with depletion of a control gene, *yellow* (*y*) (Fig. 2A–C, G). Ctrip knockdown also decreased the levels of endogenous *notum* (Notum-HA; Supplementary Fig. 6)[38]. Ctrip depletion did not disrupt *wingless* expression (Supplementary Fig. 7A–L), indicating that this defect in Wingless transduction resulted from decreased signaling downstream of Wingless. The expression of Notch and Hedgehog target genes was not reduced by Ctrip depletion (Supplementary Fig. 7A–X), ruling out generalized effects on signaling. These conclusions were also supported by tissue-specific CRISPR/Cas9-mediated *ctrip* mutagenesis[39]. Expression of *Cas9* and *ctrip* single guide RNAs (sgRNAs) in the posterior compartment of the wing disc decreased Ctrip levels efficiently (Supplementary Fig. 8D, G), and resulted in *sens* reduction (Supplementary Fig. 8E, H, J), by contrast with the control *ebony (e)* sgRNAs (Supplementary Fig. 8A, B, J). These findings were further supported by analyses in the adult wing, in which inactivation of Wingless/Wnt signaling disrupts patterning at the periphery, resulting in aberrant notch formation at the wing margin[40]. Depletion of Ctrip using multiple RNAi constructs resulted in notches at the wing margin (Fig. 2J–N), as does knockdown of the Wingless receptor

https://doi.org/10.1038/s41467-025-60535-5

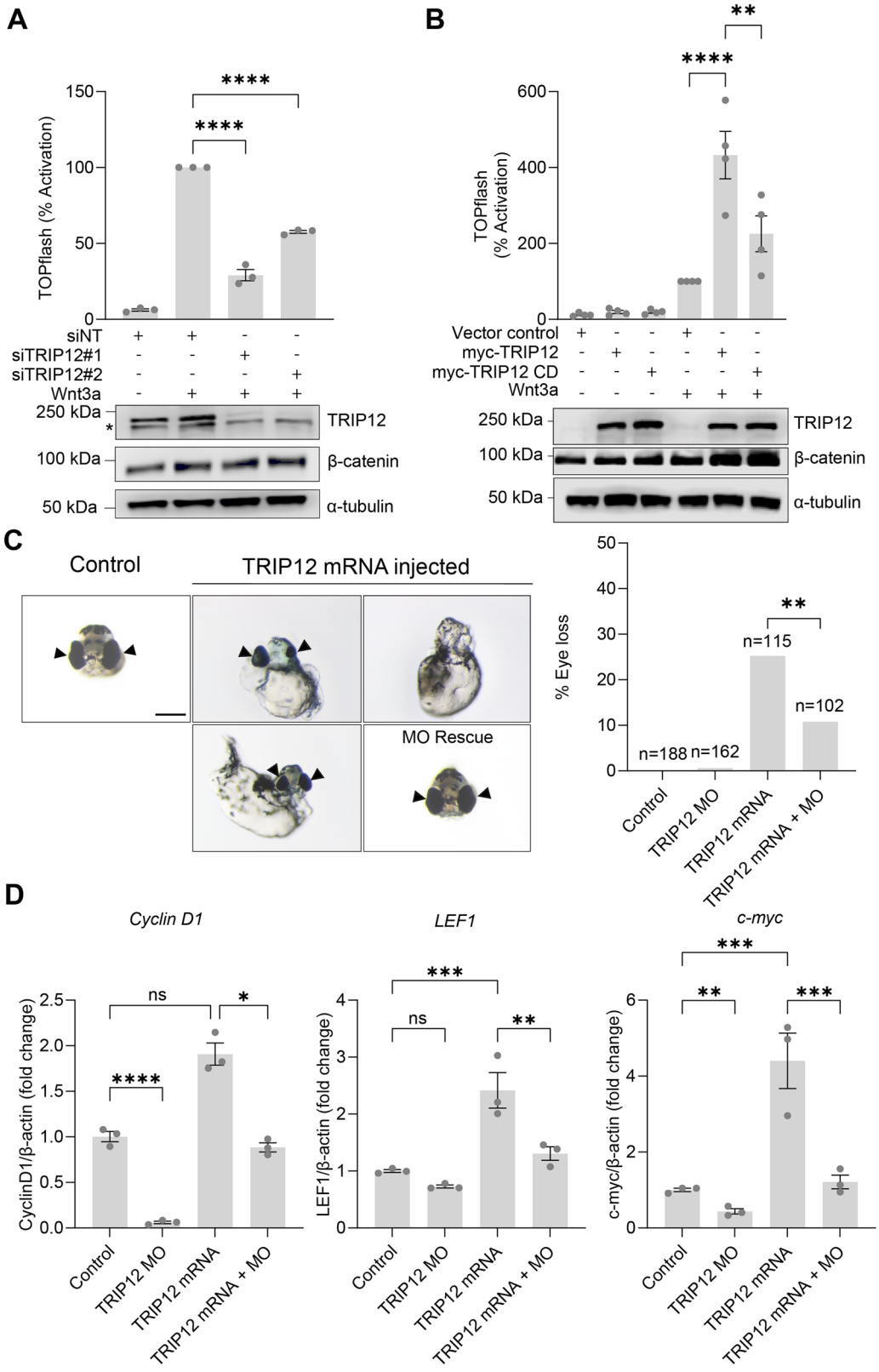

Arrow/LRP6 (Fig. 2I, N). Together, these findings provide evidence that Ctrip promotes Wingless signaling.

To determine whether Ctrip mediates other physiological events directed by the Wingless morphogen, we analyzed the *Drosophila* adult intestine, in which Wingless directs patterning at compartment boundaries, including the midgut-hindgut boundary (MHB)[41,42]. Transcriptional activation of the Wingless target gene *frizzled 3* (*fz3*)[43,44] is highest near the Wingless source at the MHB and decreases in a graded manner with increasing distance from this source[41,42]. As expected, RNAi-mediated knockdown of Arrow/LRP6 using *caudal (cad)-Gal4*, which drives strong expression near the MHB and in the posterior half of the posterior midgut (Supplementary Fig. 9A, B), resulted in a reduction of *fz3-GFP* near the MHB (Fig. 2Q, R, U). Similarly, Ctrip depletion with multiple RNAi constructs also reduced *fz3-GFP* near the

Fig. 1 | TRIP12 promotes Wnt signaling in human cells and zebrafish. **A** HEK293STF cells were transfected with nontargeting (siNT) or two independent TRIP12 siRNAs (siTRIP12#1 and #2) and incubated in the presence or absence of recombinant Wnt3a. TOPflash reporter activity quantified, and cell extracts immunoblotted for TRIP12 and β-catenin. α-tubulin is a loading control. *indicates a nonspecific band. Graphs show mean ± SEM of TOPflash normalized to cell number and control. Significance assessed using one-way ANOVA with Dunnett's test. *p*-values for siNT + Wnt3a versus siTRIP12#1 and siTRIP12#2 are <0.0001. TOPflash and immunoblots represent at least three independent experiments. $n = 3$ wells of cells per treatment group per experiment, as shown in the dot plot. **B** HEK293STF cells transfected with empty vector control or plasmids encoding Myc-TRIP12 wild-type (WT) or Myc-TRIP12 catalytic-dead (CD) and incubated in the presence or absence of recombinant Wnt3a. TOPflash reporter activity quantified, and cell extracts immunoblotted for TRIP12 and β-catenin. α-tubulin is a loading control. Graphs show mean ± SEM of TOPflash normalized to cell number and control. Significance assessed with one-way ANOVA with Tukey's test. *p*-value for myc-TRIP12 + Wnt3a versus control +Wnt3a is <0.0001 and for myc-TRIP12 + Wnt3a versus myc-TRIP12 CD + Wnt3a is 0.0028. **C** Zygotes injected with TRIP12 mRNA. Rescues were co-injected with TRIP12 MO. Representative images are shown on the left, with arrows indicating developing eyes. The percentage of eyeless embryos is graphed on the right. Scale bar = 200 mm. Significance analyzed by Fisher's exact test (two-sided), *p*-value is 0.0081. **D** Co-injection with mRNA and MO rescues expression of *Cyclin D1*, *Lef1*, and *c-myc*. Total mRNAs isolated from injected single embryos, and *Cyclin D1*, *Lef1*, and *c-myc* levels quantified by RT-qPCR. Gene expression is graphed as ratio to β-actin control and normalized to uninjected embryo controls. Graphs show mean ± SEM, $n = 3$ independent embryo pools. Significance assessed using one-way ANOVA with Tukey's test. *p*-values for Control versus TRIP12 MO, Control versus TRIP12 mRNA, TRIP12 mRNA versus TRIP12 mRNA + MO are 0.0000085, 0.092147, 0.0430227 for *Cyclin D*, 0.0947633, 0.0003199, 0.0033959 for *Lef1*, 0.0072358, 0.0002207, 0.0005341 for *c-myc*. $^{*}p < 0.05$, $^{**}p < 0.01$, $^{***}p < 0.001$, $^{****}p < 0.0001$, $p \geq 0.05$ not significant (ns). Source data provided.

MHB (Fig. 2S–U and Supplementary Fig. 9F–N). Together, these findings indicate that Ctrip promotes Wingless signaling in multiple physiological contexts.

The E3 ligase activity of TRIP12 is required for its Wnt signaling function, and acts downstream of the β-catenin destruction complex

We next addressed the mechanism of action of TRIP12 in the Wnt pathway. As TRIP12 is an E3 ubiquitin ligase, we tested whether its ligase activity is required for its role in Wnt signaling and found that overexpression of a "catalytic-dead" form of TRIP12 (TRIP12-CD) markedly reduced ability to promote Wnt3a-mediated signaling (Fig. 1B, Supplementary Fig. 10A). This mutant form of TRIP12 weakly activated Wnt signaling, suggesting that it could act as a scaffold protein or retain residual enzymatic activity (Fig. 1B). These results indicate that TRIP12 requires catalytic activity for its full function in the Wnt pathway. The expression of a TRIP12 mutant that is unable to bind poly(ADP-ribose) polymerase (PARP)[45] activated Wnt signaling at levels comparable to wild-type TRIP12, suggesting that the PARP binding domain of TRIP12 is dispensable for its Wnt activity, at least when overexpressed (Supplementary Fig. 10B). No observable change in β-catenin levels was detected when TRIP12 was knocked down or overexpressed, suggesting that TRIP12 functions downstream of β-catenin stabilization (Fig. 1A, B and Supplementary Fig. 10). Consistent with this conclusion, we found that TRIP12 localized primarily in the nucleus, and no observable change in localization was detected upon Wnt stimulation by immunostaining (Supplementary Fig. 11A) or biochemical fractionation (Supplementary Fig. 11B). We observed similar nuclear enrichment of *Drosophila* Ctrip (Supplementary Fig. 11C–H). Knockdown of Axin and APC, components of the β-catenin destruction complex, results in stabilization of β-catenin and Wnt pathway activation. Concomitant knockdown of TRIP12 reduced Wnt reporter activity in both cases (Fig. 3A, B). These results further supported a role for TRIP12 downstream of the β-catenin destruction complex to mediate nuclear Wnt signaling. To explore this possibility further in an ex vivo system, we tested whether downregulating TRIP12 affected the growth of organoids from APC^{min} mice, which do not require exogenous Wnt ligands for growth[46]. We found that TRIP12 knockdown by shRNA lentivirus treatment decreased organoid size and promoted cell differentiation, as reflected by the formation of multiple protrusions reminiscent of crypt-like structures seen in wild-type enteroids and expression of the differentiation marker *Muc2* (Fig. 3C–G, Supplementary Fig. 11I–K), supporting a role for TRIP12 downstream of APC.

Further evidence that TRIP12 acts downstream of the destruction complex was provided by genetic epistasis experiments in *Drosophila*, using either *Apc1* knockdown or a constitutively activated Armadillo/β-catenin. The activation of Wingless signaling resulting from *Apc1* depletion in the adult midgut is known to result in hyperproliferation of intestinal stem cells (ISCs), leading to an increase in stem and progenitor cell number (Fig. 4B, F)[42,47,48]. Concomitant RNAi-mediated knockdown of *Apc1* and *ctrip* in intestinal stem and progenitor cells using the temperature-sensitive *escargot* (esg^{ts})-*Gal4* driver resulted in a reduction in stem and progenitor cells (Fig. 4D–F), in contrast with concomitant RNAi-mediated knockdown of *Apc1* and *wingless* (Fig. 4C, F). These findings support the conclusion that *Ctrip* acts downstream of APC and the destruction complex. To further test this conclusion, we tested a constitutively active form of Armadillo/β-catenin (Arm^{S10}), which encodes an amino-terminal truncation that prevents its phosphorylation by the destruction complex[49]. Expression of arm^{S10} in the wing disc using the *vestigial B (vgB)-Gal4* driver resulted in an increased number of Sens-positive cells, demonstrating the expected constitutive activation of Wingless signaling (Fig. 4G–J). Concomitant depletion of *ctrip* reduced Sens (Fig. 4G, K–P), indicating that *ctrip* acts downstream of the β-catenin destruction complex. In contrast, neither Hedgehog nor Notch-dependent target gene activation was disrupted, ruling out a generalized disruption in transcription or wing disc patterning (Supplementary Fig. 12). These in vivo findings support the conclusion that TRIP12/Ctrip acts downstream of the β-catenin destruction complex.

TRIP12 interacts with the SWI/SNF catalytic component BRG1

To identify interactors of TRIP12 that mediate its role in activating Wnt signaling, we generated HEK293T cells stably transfected with TRIP12 or a catalytically compromised version ($TRIP12^{C2007A}$) fused to the turboID biotin ligase and tagged with a 3xFLAG-epitope for co-immunoprecipitation and proximity labeling[50]. Briefly, cells stably expressing 3xFLAG-TurboID-$TRIP12^{C2007A}$, which was used to stabilize protein interactions, were treated with biotin, biotinylated proteins were enriched with streptavidin beads, and subsequently analyzed via quantitative label-free mass spectrometry (MS). As we observed non-specific labeling of TRIP12 occurring in the absence of biotin treatment (due to the presence of endogenous biotin), cells that had not been treated with biotin were used as a negative control for comparison (Fig. 5A). In parallel, we performed FLAG affinity purification coupled to MS (AP/MS) as an orthogonal approach to identify interactors of $TRIP12^{C2007A}$ (Fig. 5B). Immunoblots from these cell lysates revealed that the levels of Turbo-ID TRIP12 and the catalytically compromised Turbo-ID TRIP12 are lower than endogenous TRIP12. Therefore, the total increase in TRIP12 levels is less than two-fold (Fig. 5C). Known TRIP12 substrates, including PARP1, Ubiquitin Specific Peptidase 7 (UBP7/USP7), and the SWI/SNF chromatin remodeling complex component BAF57 (SMCE1), were amongst the 358 proteins identified as putative TRIP12 interactors using both proximity labeling and FLAG AP-MS approaches (Fig. 5C, Supplementary Data 1)[45,51–53]. Other members of SWI/SNF chromatin remodeling complexes were also

https://doi.org/10.1038/s41467-025-60535-5

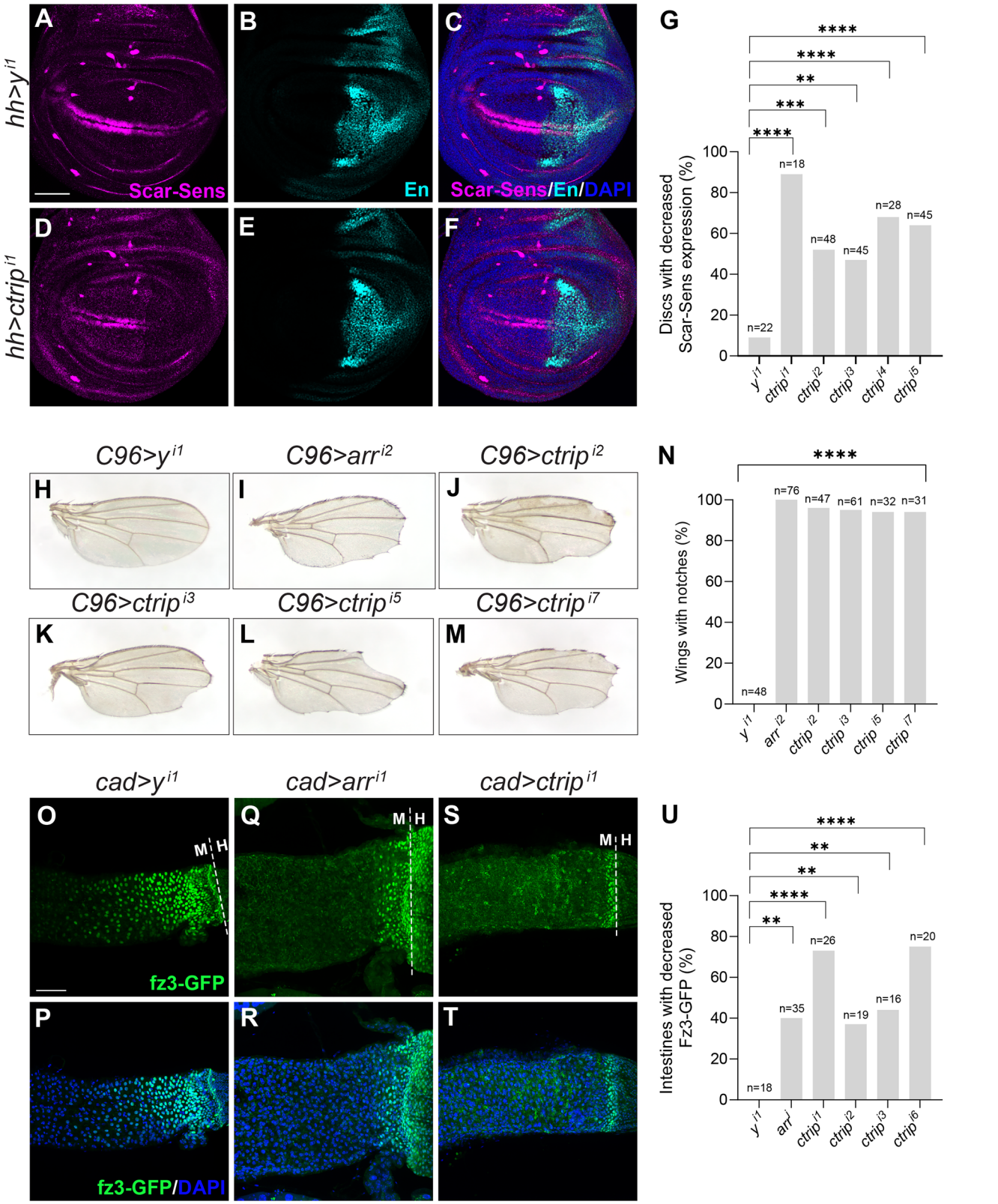

identified, consistent with an over-representation analysis (ORA) of significant proteins, which revealed chromatin assembly and disassembly machinery as the highest Gene Ontology (GO) term (Fig. 5D). Of note, TRIP12 interacted with the catalytic subunit of the SWI/SNF complex, Brahma-related gene 1 (BRG1/SMARCA4), a known nuclear regulator of Wnt signaling[13]. Supporting these MS results, we found that overexpressed (Supplementary Fig. 13A, B) and endogenous (Fig. 5E, Supplementary Fig. 13C) BRG1 and TRIP12 co-immunoprecipitate in a Wnt-independent manner. A proximity ligation assay confirmed their association, providing further support that their interaction is direct and Wnt-independent (Fig. 5F, G, Supplementary Fig. 14).

Fig. 2 | Ctrip promotes Wingless signaling in *Drosophila*. RNAi constructs targeting *yellow* negative control or *ctrip* in the posterior compartment (marked by Engrailed (En, cyan)) of third instar larval wing discs using *hedgehog (hh)-Gal4*. *Scarlet-Senseless* (Scar-Sens, magenta) is a Wingless target gene reporter. DAPI (blue) marks nuclei. Scale bar (**A**–**F**): 50 µm. Dorsal, top; posterior, right. **A**–**C** *hh-Gal4*-driven expression of a *yellow (y)* RNAi control. Minimal loss of Scar-Sens was observed in the posterior compartment. **D**–**F** *hh-Gal4*-driven expression of RNAi construct targeting *ctrip* decreases Scar-Sens in the posterior compartment. **G** Quantification is the percentage of wing discs with decreased Scar-Sens. *N* is the number of wing discs analyzed. RNAi constructs targeting *yellow*, *arrow* (positive control), or *ctrip* expressed using the *C96-Gal4* driver. **H** *C96-Gal4*-driven expression of RNAi construct targeting *yellow (y)*. No wing notches were observed. **I**–**M** *C96-Gal4*-driven expression of RNAi constructs targeting *arrow (arr)* or *ctrip* resulted in notches at wing periphery. **N** Quantification for **H**–**M** is shown as percentage of wings with notches. *N* is the number of wings analyzed. RNAi constructs targeting *yellow*, *arrow (arr)*, or *ctrip* expressed in posterior midgut using the *cad-Gal4* driver. *frizzled3-GFP* (green) is a Wingless target gene reporter. The dashed line indicates the midgut-hindgut boundary (MHB). **O**, **P** *cad-Gal4*-driven expression of *y*. No *fz3-GFP* reduction was observed. **Q**, **R** *cad-Gal4*-driven expression of RNAi targeting *arr* results in loss of *fz3-GFP* near midgut-hindgut boundary. **S**, **T** *cad-Gal4*-driven expression of RNAi targeting *ctrip* results in partial or complete loss of *fz3-GFP* expression in posterior midgut. DAPI (blue) marks nuclei. Scale bar (**O**–**T**): 50 µm. **U** Quantification shown as percentage of intestines with decreased *fz3-GFP*. *N* is the number of adult intestines analyzed. Statistical significance (**G**, **N**, **U**) was analyzed by Fisher's exact test (two-sided). *p*-values for **G** are <0.0001, 0.0005, 0.0024, <0.0001, <0.0001 respectively. *p*-values for **N** are all <0.0001. *p*-values for **U** are 0.0020, <0.0001, 0.0080, 0.0021, <0.0001, respectively. $^{**}p < 0.01$, $^{***}p < 0.001$, $^{****}p < 0.0001$. Source data are provided in the Source Data file.

BRG1 is required for TRIP12-dependent Wnt signaling in human cells and *Drosophila*

BRG1 has been shown to positively (via binding to β-catenin)[13,54,55] and negatively[56,57] regulate Wnt signaling. Thus, it is possible that the effects of the SWI/SNF complex on Wnt signaling are tissue- or context-dependent. We found that BRG1 knockdown in human HEK293T cells with three independent siRNAs blocked Wnt3a-induced signaling (Fig. 6A), indicating a positive role for BRG1. To test whether BRG1 is required for TRIP12-mediated Wnt signaling, we knocked down BRG1 in HEK293STF cells overexpressing TRIP12. We found that Wnt pathway activation upon TRIP12 overexpression was inhibited by knocking down BRG1 (Fig. 6B), indicating a requirement for BRG1 in TRIP12-mediated Wnt signaling.

We found that BRG1 is also required for Wingless signaling in vivo. The closest relative of human BRG1 is encoded by a single *Drosophila melanogaster* gene, *brahma (brm)*, which shares 81% amino acid similarity with human BRG1. We found that RNAi-mediated Brm depletion with independent RNAi constructs resulted in reduction or loss of endogenous GFP-tagged Brm (Brm-GFP) (Supplementary Fig. 15). Strong Brm knockdown resulted in mildly deformed wing discs whereas complete loss of Brm prevented wing development (Supplementary Fig. 15D–I). Brm knockdown in the posterior compartment using the *hh-Gal4* driver resulted in loss of the Wingless target genes *sens* and *notum*, in contrast with knockdown of the *y* control (Fig. 6C–I, Supplementary Fig. 16). Similarly, RNAi-mediated depletion of other SWI/SNF complex subunits (Osa/BAF250A/B and Bicra/BICRAL) also resulted in *sens* reduction (Supplementary Figs. 17, 18). In contrast, expression of a Hedgehog target gene (*patched*) and a Notch target gene (*wingless*) were not reduced (Supplementary Figs. 19–21), ruling out a generalized disruption of cell signaling, transcription, or wing patterning. Similarly, in the adult intestine, RNAi-mediated depletion of Brm resulted in the reduction of *fz3-GFP* expression near the MHB (Fig. 6L–P). These findings demonstrate that SWI/SNF complexes promote Wingless signaling in multiple physiological contexts.

TRIP12 ubiquitylates BRG1 in cells and in vitro

As TRIP12 binds BRG1, we sought to determine if BRG1 is a TRIP12 ubiquitylation substrate. We used a maltose-binding protein (MBP) tandem ubiquitin-binding entities (TUBE) fusion protein to isolate polyubiquitylated proteins, followed by immunoblotting. Overexpression of TRIP12 in the presence of Wnt3a enhanced the ubiquitylation of endogenous BRG1, indicating that TRIP12 promotes BRG1 polyubiquitylation in a Wnt-dependent manner (Fig. 7A). In contrast, no increase in BRG1 ubiquitylation was observed with overexpression of TRIP12 alone. Consistent with this conclusion, BRG1 ubiquitylation was not increased when the catalytic-dead TRIP12 mutant was overexpressed at a similar level in the presence of Wnt3a (Fig. 7B). To further test the effect of TRIP12 on the ubiquitylation of BRG1, we used an independent approach, the NanoBiT luciferase-based complementation (HiBiT) system. In this system, the holo, active nanoluciferase protein is reconstituted when proteins tagged with the HiBiT fragment and the LgBiT fragment are in proximity[58]. Co-overexpression of a *HiBiT-tagged BRG1* construct with an *LgBiT-tagged ubiquitin* construct in HEK293T cells resulted in a luminescent signal, indicative of a close association between the two proteins (Supplementary Fig. 22A, B). The nanoluciferase signal decreased when TRIP12 was knocked down with siRNA (Supplementary Fig. 22B), suggesting an inhibition of BRG1 ubiquitylation. Similarly, BRG1 ubiquitylation was reduced with TRIP12 knockdown in an HA-tagged ubiquitin assay (Fig. 7C), whereas TRIP12 overexpression again enhanced BRG1 ubiquitylation (Supplementary Fig. 22C). To more directly assess whether BRG1 is a substrate of TRIP12, we performed an in vitro ubiquitylation assay using recombinant BRG1 protein and BRG1 isolated from HEK293 cells and found that BRG1 is a direct substrate of TRIP12 (Fig. 7D, Supplementary Fig. 22D). Additionally, we found that TRIP12 preferentially adds K63-Ub chains to BRG1 (Supplementary Fig. 22E)[52,59,60]. No ubiquitylation of MBP was observed with the addition of TRIP12 (Supplementary Fig. 22F). These findings and our demonstration that the ligase activity of TRIP12 is required for its full Wnt activity (Fig. 1B, Supplementary Fig. 10A) support the conclusion that TRIP12 ubiquitylates BRG1 to promote Wnt signaling.

TRIP12 enhances BRG1 capacity to bind β-catenin in the presence of Wnt

We next tested several hypotheses for how TRIP12-mediated BRG1 ubiquitylation promotes Wnt signaling. The effect of TRIP12 on the BRG1 ubiquitylation state parallels its effect on Wnt reporter activity. Because protein ubiquitylation often serves as a signal for proteasomal degradation, we tested whether TRIP12 reduces the stability of BRG1. Ctrip knockdown in the dorsal compartment of wing discs using the *ap-Gal4* driver resulted in increased levels of endogenous BAF57 (Bap111 in *Drosophila*)[61], a known substrate[53] (Fig. 7E–G, K), but no observable change in endogenous levels of Brm (Fig. 7H–J, L). Similarly, we found that neither overexpression (Fig. 7M) nor knockdown (Fig. 7N) of TRIP12 had any observable effect on the steady-state levels of BRG1 in the absence or presence of Wnt. These findings were further supported by the observation that overexpression of TRIP12 had no effect on the turnover rate of BRG1 (Supplementary Fig. 22G). These results indicate that BRG1 ubiquitylation by TRIP12 does not affect its stability.

SWI/SNF complexes are composed of over a dozen proteins, including BRG1 and BRG1-associated factors (BAFs). We tested whether BRG1 ubiquitylation by TRIP12 affected the composition of SWI/SNF by regulating the interactions between BRG1 and BAF proteins. To test this possibility, we overexpressed BRG1 and TRIP12 in HEK293T cells and performed immunoprecipitation of BRG1, followed by MS to identify associated factors. We found that TRIP12 had little observable effect on the composition of 11 primary SWI/SNF components that

https://doi.org/10.1038/s41467-025-60535-5

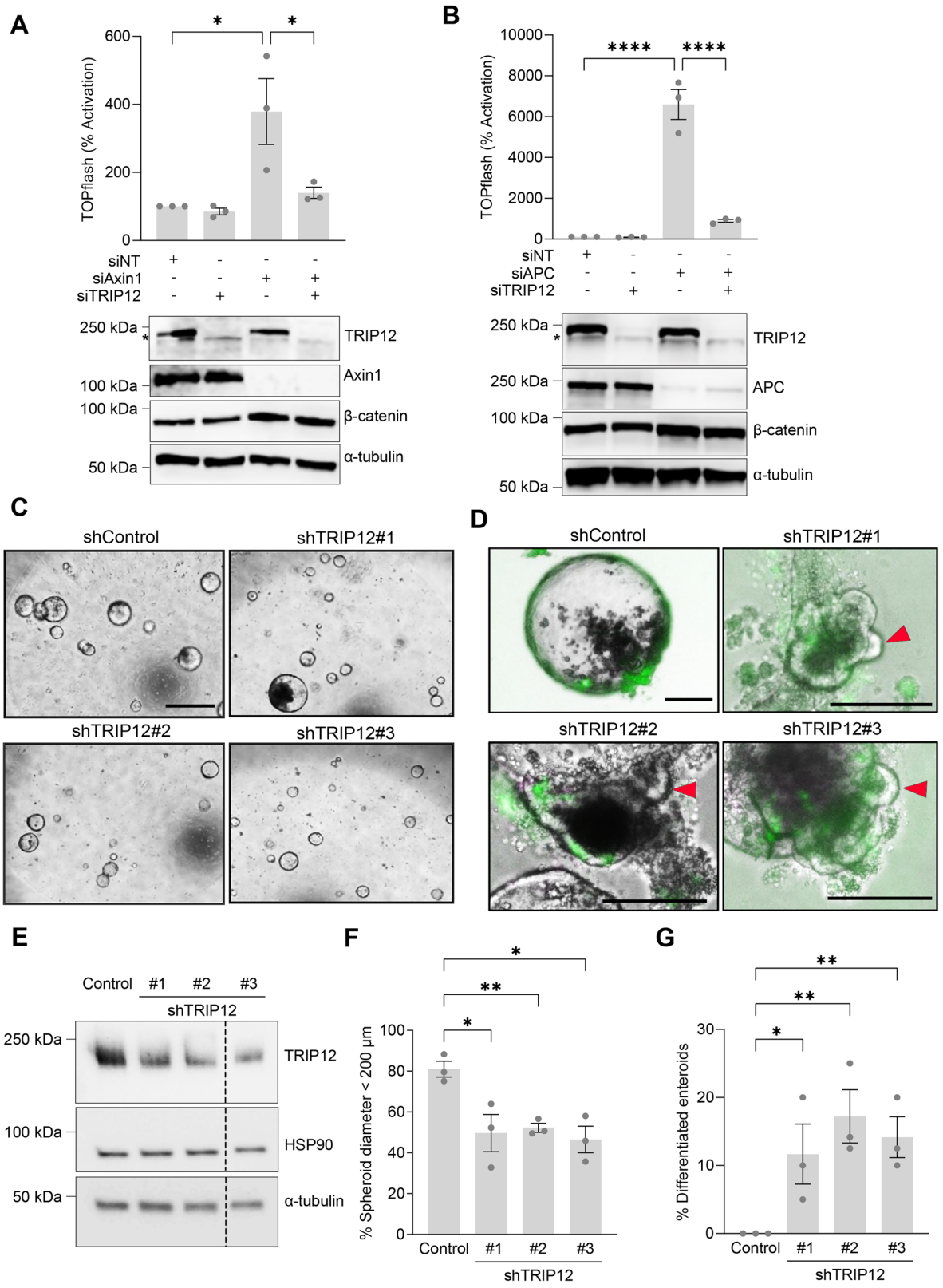

were pulled down with BRG1 (Supplementary Fig. 23, Supplementary Data 2).

We showed previously that the capacity of β-catenin to bind TCF4 is regulated by the ubiquitylation state of the corepressor, Gro/TLE[19]. Although ubiquitylation of BRG1 by TRIP12 did not appear to regulate BRG1 binding to other SWI/SNF complex components, we speculated that BRG1 ubiquitylation may affect its interaction with β-catenin. To test this possibility, we knocked down TRIP12 in HEK293T cells and assessed the binding of BRG1 to β-catenin in the absence or presence of Wnt. We found that the binding of β-catenin by BRG1, as assessed by their co-immunoprecipitation, was inhibited by knockdown of TRIP12 (Fig. 8A). Conversely, binding of β-catenin to BRG1 was increased with overexpression of wild-type TRIP12, but to a lesser extent with a catalytic-compromised TRIP12 construct, suggesting that the full

Fig. 3 | TRIP12 functions downstream of β-catenin stabilization. A HEK293STF cells were transfected as indicated with nontargeting (siNT) control, TRIP12 siRNAs, Axin siRNAs, or TRIP12 and Axin siRNAs. TOPflash reporter activity quantified, and cell extracts immunoblotted for TRIP12, Axin, and β-catenin. *indicates a non-specific band. Graphs show mean ± SEM of TOPflash normalized to cell number and control. Significance assessed using the one-way ANOVA with Tukey's test. *p*-value for siAxin1 versus siNT is 0.0167 and for siAxin1 versus siAxin1 + siTRIP12 is 0.0366. For **A** and **B**, TOPflash and immunoblots are representative of at least three independent experiments. $n = 3$ wells of cells per treatment group per experiment. α-tubulin is loading control. **B** HEK293STF cells transfected as indicated with siNT control, TRIP12 siRNAs, APC siRNAs, or TRIP12 and APC siRNAs. TOPflash reporter activity quantified, and cell extracts immunoblotted for TRIP12, APC, and β-catenin. *indicates a nonspecific band. Significance assessed using one-way ANOVA with Tukey's test. *p*-values for siAPC versus siNT and siAPC versus siAPC + siTRIP12 are <0.0001. APC^{min} organoids infected with control shRNA (Control) or three distinct shTrip12 lentiviral particles (#1, #2, and #3), imaged, and quantified for **C, F** organoid diameter (<200 µm) after 3 days, and evidence of **D, G** differentiation (villus formation, indicated by arrowheads) after 4 days. **F**: $n > 50$ organoids per experiment, **G**: $n > 20$ organoids per experiment. Scale bar in **C** 800 µm, **D** 50 µm. **D** GFP marks lentivirus-infected cells. Graphs show mean ± SEM of three independent replicates. Significance for **F** was analyzed by two-tailed Student's *t* test and *p*-values are 0.0338, 0.0030, 0.0103, respectively. Significance for **G** was analyzed by one-tailed Student's *t* test and *p*-values are 0.0286, 0.0058, 0.0046, respectively. **E** Immunoblotting was performed to confirm reduction in TRIP12 levels. HSP90 and α-tubulin are loading controls. Representative images are shown ($n = 3$ independent experiments). The dashed line between #2 and #3 represents intervening wells. $^{*}p < 0.05$, $^{**}p < 0.01$, $^{****}p < 0.0001$. Source data are provided in the Source Data file.

catalytic activity of TRIP12 is required to promote the binding of β-catenin to BRG1 (Fig. 8B). To further test the effect of TRIP12 on the interaction between BRG1 and β-catenin, we used an independent approach, the HiBiT system (Fig. 8C). A luminescent signal was observed when a *HiBiT-tagged BRG1* construct was co-expressed with a *LgBiT-tagged β-catenin* construct in HEK293T cells, indicating the two proteins are closely associated. The nanoluciferase signal decreased when TRIP12 was knocked down with siRNA (Fig. 8D), suggesting an inhibition of the BRG1-β-catenin interaction. Conversely, the luminescent signal increased when TRIP12 was overexpressed in the presence of Wnt3a ligand (Fig. 8E). These results provide further support for the conclusion that TRIP12 promotes the binding of β-catenin to BRG1 in the presence of Wnt (Fig. 8F).

TRIP12 is expressed in the human colon and high levels of TRIP12 in pancreatic cancer patients correlate with reduced survival

Wnt signaling is required for maintaining adult intestinal homeostasis[6]. We performed multiplex immunofluorescence on formalin-fixed, paraffin-embedded (FFPE) human tissue sections to determine if TRIP12 and BRG1 are expressed in the human colon (Supplementary Fig. 24). We found that TRIP12 and BRG1 are expressed in an overlapping pattern in the human colon, with BRG1 staining exclusively in the nucleus. Although predominantly nuclear, faint staining of TRIP12 was also observed in the cytoplasm. TRIP12 and BRG1 appeared concentrated in the crypts. Given the role of Wnt signaling as an oncogenic pathway, we asked whether TRIP12 is altered in human cancers. We found that the *TRIP12* gene is mutated in several tumor types, with the *TRIP12* mRNA level relative to the corresponding normal tissue dependent on cancer type[32]. Specifically, using data from the Cancer Genome Atlas[62,63], we found that high expression of *TRIP12* mRNA was correlated significantly with a reduced survival of patients with pancreatic adenocarcinoma (Supplementary Fig. 25), a cancer associated with activated Wnt signaling[64].

Discussion

Herein, we identify TRIP12 as a positive regulator of Wnt signaling. Our findings from multiple model systems indicate that the role of TRIP12 in Wnt signaling is conserved across metazoans. Conversion of chromatin from a repressive to a permissive state is critical for regulating gene transcription in many signaling pathways, but our understanding of how this switch occurs is limited. For Wnt signaling, we propose a model in which BRG1, a catalytic ATPase of the SWI/SNF complex, is ubiquitylated by TRIP12, which increases its association with nuclear β-catenin. Alternatively, the SWI/SNF complex may be recruited to β-catenin-bound TCF/Lef sites. Ubiquitylation has been shown to regulate the stability of the SWI/SNF complex through a quality-control mechanism that promotes the degradation of incomplete SWI/SNF complexes and by altering the kinetics of gene transcription[65,66]. Our finding that TRIP12 ubiquitylates BRG1 provides a novel example of a ubiquitin ligase-directed mechanism that targets the SWI/SNF chromatin remodeling complex to regulate signal pathway-dependent transcription. Consistent with our findings, the depletion of TRIP12 in planarians was shown to prevent the specification and maintenance of posterior tissues during homeostasis and regeneration, phenotypes consistent with Wnt pathway inhibition[67].

TRIP12 has been implicated in chromatin regulation through several mechanisms. TRIP12 ubiquitylates several proteins that regulate chromatin modification and transcription, including RNF168 and ARF. The E3 ligase RNF168 ubiquitylates histone H2A and H2AX at sites of DNA damage, promoting the recruitment of DNA repair proteins. Ubiquitylation of RNF168 by TRIP12 targets RNF168 for proteasomal degradation, preventing the spread of RNF168-mediated chromatin ubiquitylation to undamaged DNA[68,69]. TRIP12 promotes the turnover of p53 as well. Ubiquitylation of the MDM2 inhibitor, ARF, by TRIP12 leads to ARF degradation. Consequently, MDM2, an E3 ligase for p53, is stabilized and p53 is degraded[70]. TRIP12 also regulates the stoichiometry of the SWI/SNF complex by controlling the level of free, unbound BAF57[53]. Our finding that TRIP12 ubiquitylates BRG1 expands our understanding of TRIP12-dependent regulation of chromatin-associated complexes.

We speculate that a similar mechanism for recruiting SWI/SNF complexes to the target genes of other signaling pathways may occur; activation of the signaling pathway would lead to increased association, via post-translational modification, of a SWI/SNF complex component with a signal pathway-specific transcriptional regulator, allowing targeting of SWI/SNF for pathway-directed transcription. Evidence consistent with this notion comes from studies demonstrating the association between the SWI/SNF subunit, BAF57, with activated androgen and estrogen nuclear receptors[71,72], and between BRG1 with the ligand-bound estrogen receptor in human cells[73]. Thus, strategies that promote the interaction between the SWI/SNF complex and transcription factors may provide an attractive approach to selectively activate pathway-specific transcriptional programs.

Whereas our findings reveal an important role for TRIP12 in the activation of Wnt signaling, several outstanding questions remain. How does Wnt stimulation induce the activity of TRIP12 toward BRG1? How does ubiquitylation promote the interaction between BRG1 and β-catenin? Is TRIP12 required for Wnt signaling in all cellular contexts or only a subset?[74] Does BRG1 also bind transcription factors from other signaling pathways to confer specificity?

Our findings may have clinical relevance, as both TRIP12 and BRG1 are mutated in human cancers[32,75]. Several clinical trials for BRG1-mutated cancers are currently ongoing[76]. Drug development for BRG1 has focused on allosteric inhibitors, inhibitors of ATPase activity, PROTACS, and bromodomain inhibitors; all have exhibited anti-proliferative effects in vitro or in mouse tumor studies[77,78]. Our study predicts that drugs that disrupt the TRIP12-BRG1 interaction would block signaling in the majority of Wnt pathway-dependent cancers. Drugs targeting TRIP12 itself represent particularly promising anti-cancer agents, given TRIP12's roles in the DNA damage response,

https://doi.org/10.1038/s41467-025-60535-5

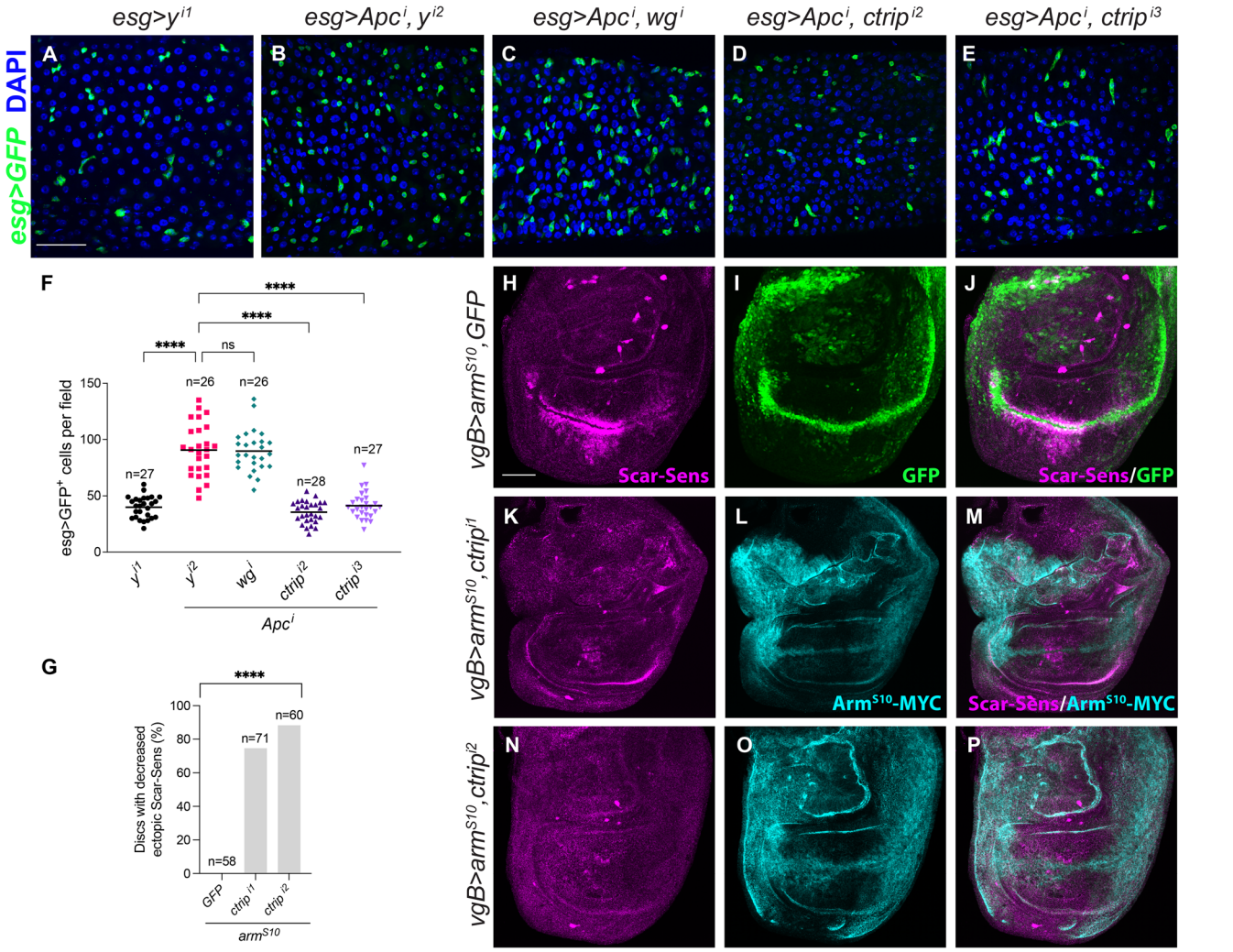

Fig. 4 | Ctrip acts downstream of β-catenin in *Drosophila*. By comparison with control (**A**, **F**), RNAi-mediated depletion of Apc1 in ISCs during pupation using the esg^{ts} (temperature-sensitive driver) leads to an increase in progenitor cell (green) number in the midgut (R5A region) (**B**, **C**, **F**). Concomitant expression of the *Apc1* RNAi construct with the *ctrip* RNAi construct leads to a significant reduction in progenitor cell number (**D**, **E**, **F**), in contrast with expression of an RNAi construct targeting *yellow* (**B**, **F**). Graphs show mean ± SEM, with all data points represented. Significance was assessed using the one-way ANOVA comparing all genotypes to control (y^{i2} + Apc^i), with Dunnett's multiple comparisons test. *N* is the number of adult intestines analyzed. *p*-values for y^{i2} + Apc^i versus y^{i1}, wg^i + Apc^i, $ctrip^{i2}$ + Apc^i, $ctrip^{i3}$ + Apc^i are <0.0001, 0.9985, <0.0001, <0.0001, respectively. Progenitor cells are marked with *esg* > *GFP* (green) and nuclei are marked with DAPI (blue). Scale bar (**A**–**E**): 50 µm. **G** Quantification is shown as the percentage of wing discs of each genotype with decreased ectopic Scar-Sens for **H**–**P**. *N* is the total number of wing discs analyzed from three independent biological replicates. Statistical significance was analyzed by Fisher's exact test (two-sided). *p*-values are both <0.0001. **H**–**P** Representative confocal immunofluorescence images of constitutively active arm^{S10} and *GFP* or RNAi constructs targeting *ctrip* were expressed in the wing pouch of third instar larval wing discs using the *vgB-Gal4* driver. *Scarlet-Senseless* (Scar-Sens, magenta) is a Wingless target gene reporter, Arm^{S10}-Myc (cyan), GFP (green). Scale bar (**H**–**P**): 50 µm. Dorsal, top, and posterior, right. **H**–**J** Representative confocal immunofluorescence images of *vgB*-driven arm^{S10} and *GFP* overexpression in wing pouch, which induces ectopic Scar-Sens positive cells. **K**–**P** Representative confocal immunofluorescence images of co-expression of arm^{S10} and RNAi against *ctrip*, which suppresses ectopic Scar-Sens-positive cells. ****$p < 0.0001$, $p \geq 0.05$ is not significant (ns). Source data are provided in the Source Data file.

maintaining low levels of p53, and, as our study shows, promoting Wnt signaling.

Methods

For the study with normal human intestinal tissue, IRB approval was obtained through Vanderbilt University Medical Center Institutional Review Board (IRB#231475). All zebrafish were treated in accordance with the University of Maryland School of Medicine's and Michigan State University's Institutional Animal Care and Use Committees. IACUC protocol number: PROTO202300374.

Drosophila stocks and genetics

Fly crosses with the *C96-Gal4* or *cad-Gal4* drivers were performed at 29 °C, other crosses were performed at 25 °C. Crosses using the temperature-sensitive progenitor cell driver esg^{ts} were maintained at 18 °C until the late third instar larval stage, then shifted to 29 °C.

Reporters: *mScar:T2A:sens*[19], *fz3-GFP*[79].

RNAi lines and Gal4 drivers

The RNAi lines $ctrip^{i1}$ (Bloomington *Drosophila* Stock Center (BDSC #33435)), $ctrip^{i2}$ (Vienna *Drosophila* Resource Center (VDRC) # 33952), $ctrip^{i3}$ (VDRC # 108546), $ctrip^{i4}$ (VDRC # 50189), $ctrip^{i5}$ (VDRC # 50190), $ctrip^{i6}$ (BDSC # 44481), $ctrip^{i7}$ (VDRC#49703), brm^{i1} (BDSC #31712), brm^{i2} (BDSC #35211), arr^{i1} (VDRC #6708), arr^{i2} (VDRC#36286), osa^{i1} (BDSC #35447), osa^{i2} (BDSC #38285), $Bicra^{i1}$ (BDSC #42847), $Bicra^{i2}$, y^{i1} (VDRC #106068) and y^{i2} (BDSC#364527) were expressed in third instar larval wing discs or intestine using *hh-Gal4* (10678169) with or without *UAS-dcr2* (BDSC #25757), or *C96-Gal4* (BDSC #43343) with *UAS-dcr2*, or

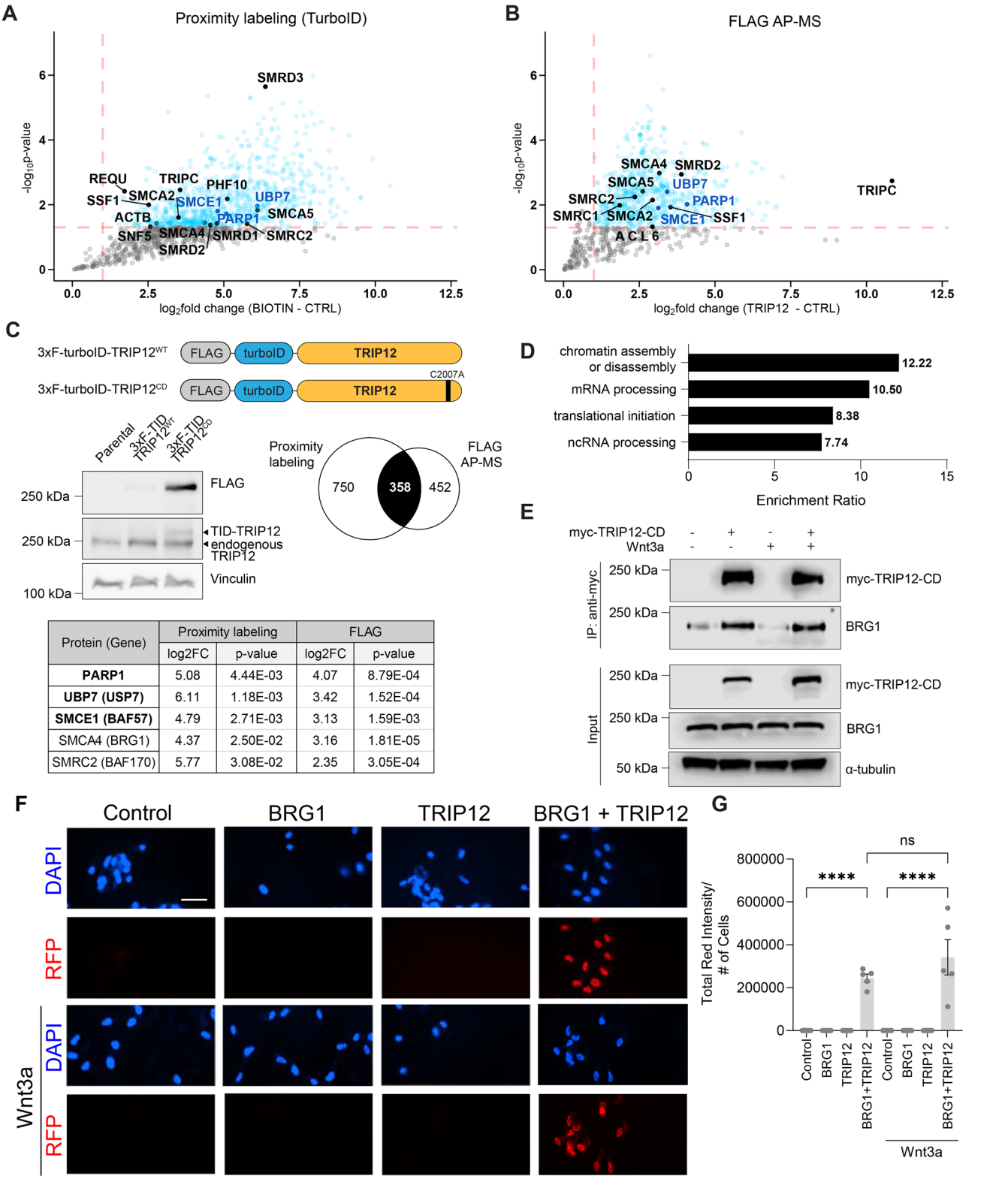

Protein (Gene)	Proximity labeling		FLAG	
	log2FC	p-value	log2FC	p-value
PARP1	5.08	4.44E-03	4.07	8.79E-04
UBP7 (USP7)	6.11	1.18E-03	3.42	1.52E-04
SMCE1 (BAF57)	4.79	2.71E-03	3.13	1.59E-03
SMCA4 (BRG1)	4.37	2.50E-02	3.16	1.81E-05
SMRC2 (BAF170)	5.77	3.08E-02	2.35	3.05E-04

ap-Gal4 (BDSC #3041), or *cad-Gal4* (BDSC #3042), or *vgB-Gal4* (gift from Andrew Tomlinson, Columbia University) or *esg-Gal4 tubGal80^{ts}* (gift from Julia Cordero, University of Glasgow).

Other stocks

ctrip$^{MI14762\text{-}GFSTF}$/TM3, Sb (BDSC#65343), *brm$^{MI01941\text{-}GFSTF}$/TM6C, Sb Tb* (BSDC #59784), *Bap111-GFP. FPTB (BDSC#64799), UAS-arm^{S10}* [49] *notum-HA*[38], and *UAS-GFP-lacZ (nls)* (BDSC#6452).

Generation of tissue-specific CRISPR mutations

CRISPR target sites were identified using http://targetfinder.flycrispr.neuro.brown.edu/. gRNA sequences are listed below. Two guide RNAs for each gene were cloned into the *pCFD6: UAS t::gRNA* plasmid. Plasmids were injected by BestGene and integrated at the *attP40* site. Wing-specific mutations were generated by crossing the gRNA-containing lines to *w; UAS-uMCas9/CyO; mScar:T2A:sens hh-Gal4 /TM6B*.

Fig. 5 | TRIP12 interacts with BRG1. A Volcano plot of significantly enriched proteins in proximity labeling of 3xFLAG-turboID-TRIP12^{C2007A}. HEK293T cells were treated with biotin or not and analyzed using label-free LC-MS/MS. Proteins with a change of greater than 1.5-fold (log2 > 0.6), $p < 0.05$ ($n = 3$ independent biological replicates, two-tailed t-test) in ±biotin comparison are in cyan. For **A** and **B**, proteins in dark blue are known interactors of TRIP12, and proteins in black are known components of SWI/SNF. **B** Volcano plot of significantly enriched proteins in 3xFLAG-TRIP12^{C2007A} immunoprecipitation versus control and analyzed by AP/MS. Proteins with a change of greater than 1.5-fold (log2 > 0.6), $p < 0.05$ ($n = 3$ independent biological replicates, two-tailed t-test) in 3x-FLAG-TRIP12^{C2007A}/control comparison are in cyan. **C** Schematic of N-terminal 3xFLAG-turboID biotin ligase-tagged TRIP12^{WT} and catalytically inactive TRIP12^{C2007A} and their immunoblot in HEK293T cell lysates. Venn diagram comparing TRIP12 interactors identified by proximity labeling and AP/MS. Among the commonly identified proteins were the known TRIP12 interactors PARP1, USP7, and BAF57, and SWI/SNF components BRG1 and BAF170. **D** Over-representation analysis of 358 common and specific TRIP12 interactors revealed chromatin assembly and disassembly as the most enriched gene ontology (GO) term with an enrichment ratio of 12.22, FDR < 0.05. **E** HEK293FT cells transfected with Myc-TRIP12-CD, incubated in the presence or absence of recombinant Wnt3a. Myc-TRIP12-CD immunoprecipitated with Myc antibody. Coimmunoprecipitated, endogenous BRG1 detected by immunoblotting. Immunoblots representative of at least three independent experiments. α-tubulin is a loading control. **F** RPE cells treated in the absence or presence of recombinant Wnt3a for 4 h, immunostained for BRG1 and/or TRIP12, and a proximity ligation assay performed with quantitation (**G**). $n = 5$ images. Representative images are shown ($n = 3$ independent experiments). Graph shows mean ± SEM of total red intensity normalized to cell number. Significance assessed using one-way ANOVA with Tukey's test. *p*-values for Control versus BRG1 + TRIP12 and Control + Wnt3a versus BRG1 + TRIP12 + Wnt3a are <0.0001. *p*-value for BRG1 + TRIP12 versus BRG1 + TRIP12 + Wnt3a is 0.3287. Scale bar: 50 µm. ****$p < 0.0001$, $p \geq 0.05$ is not significant (ns). Source data are provided in the Source Data file.

gRNAs for tissue-specific CRISPR mutagenesis:
ctrip Line1:
gRNA1: 5′−GTCGACGGAGGAGCTTACAG CGG−3′
gRNA2: 5′−TTGATCACTGACGACCGGTA TGG−3′
ctrip Line2:
gRNA1: 5′−GCCAAGCACAAGCAGCGCTG CGG−3′
gRNA2: 5′−GAAGAGGAGGTGGGCTTCTA CGG−3′
ebony Line3:
gRNA1: 5′−GGCTGTGTGCATGCAGCCGT CGG−3′
gRNA2: 5′−GTTCTTCACCGGACGATAGT CGG−3′

Immunohistochemistry

Third instar larvae and female adults were dissected in phosphate-buffered saline (PBS). Wing discs from 3rd instar larvae were fixed for 20 min in 4% paraformaldehyde at room temperature and female adult intestine were fixed in 4% paraformaldehyde for 45 min at room temperature. After fixation, tissues were washed 3 times for 10 min with PBS + 0.1% Triton X-100 and blocked for 1 h with PBS + 0.1% Tween 20 + 10% bovine serum albumin (BSA) at room temperature. Wing discs and intestine were incubated with primary antibody (diluted in PBS + 0.5% Triton X-100) at 4 °C overnight. Three 10 min washes and a 2 h secondary antibody incubation were carried out at room temperature. The samples were subsequently stained with 4′,-diamidino-2-phenylindole (DAPI; 2 µg/ml) and mounted in Prolong Gold Antifade Reagent (Invitrogen). Confocal images were captured on a Nikon CSU-W1 spinning disk confocal microscope, or a Yokogawa CSU-W1 SoRa spinning disk confocal microscope from Nikon and processed with Adobe Photoshop/Illustrator software.

Antibodies for immunostaining

The primary antibodies used were rabbit DsRed (1:500, 632496) from TaKaRa, rabbit anti-GFP (1:500, A11122) and chicken anti-GFP (1:500, A10262) from Thermo Fisher Scientific, rat HA (1:2000, 11867423001) from Roche, mouse anti-β-galactosidase (1:500, Z378B) from Promega, mouse Myc (1:500, 9E10) from Santa Cruz, mouse anti-Engrailed (1:100, 4D9), mouse anti-Wingless (1:500, 4D4), mouse anti-Patched (1:500, Apa1), mouse anti-LamC (1:500, LC 28.26), mouse Armadillo (1:50, N2 7A1) and mouse Cut (1:20, 2B10) from Developmental Studies Hybridoma Bank (DSHB). Secondary antibodies were goat or donkey Alexa Flour 488, 555, or 647 conjugates (1:500) from Invitrogen, and goat or donkey Cy5 conjugates (1:500) from Life Technologies/Jackson Immunochemicals.

Plasmids and purified proteins

pCS2-Myc-TRIP12 was generated by GenScript using standard PCR-based cloning strategies. pAc-GFP-TRIP12 and pAc-GFP-TRIP12-CD were gifts from Jiri Lukas (University of Copenhagen). pCMV5-BRG1-FLAG and pCS2-HA-Ub were generated using standard PCR-based cloning strategies. pMAL-C5E-6xTUBE was synthesized based on the 6xTUBE sequence by GenScript[80]. MBP-TUBE and MBP were purified according to the protocol from New England Biolabs (NEB) for pMAL-based vectors. GST-TRIP12-HECT was synthesized according to the protocol from NEB for pGEX-based vectors. pRP-BRG1-HA-HiBiT and pRP-β-catenin-V5-LgBiT were purchased from VectorBuilder. pcDNA3.1-Ub-Myc-LgBiT and pGEX-TRIP12-HECT were purchased from GeneUniversal. Recombinant murine Wnt3a protein was purchased from TIME Bioscience. Recombinant human GST-TRIP12-HECT protein (#513901, amino acids 1643-1992) was purchased from Novo-Pro. Recombinant human His-BRG1 protein was purchased from ProteinOne. pCS2-Myc-TRIP12-CD, pCS2-Myc-TRIP12-PARP, and pCS2-Myc-TRIP12-RES were generated using site-directed mutagenesis with the QuikChange II XL Site-Directed Mutagenesis kit (Agilent) with the following primers:

TRIP12-CD (C2007A):
Forward:
5′-CAACTTAAGATAGTTCACAGCAGTCATTACAGAGGGCAA-GAAGTCAT-3′
Reverse:
5′- ATGACTTCTTGCCCTCTGTAATGACTGCTGTGAACTATCTTAA GTTG-3′
TRIP12-PARP (R869A):
Forward: 5′ − CACGGGAACAGCAGCTGCCATTCAGAGAAAACC-3′
Reverse: 5′ − GGTTTTCTCTGAATGGCAGCTGCTGTTCCCGTG-3′
TRIP12-RES (A399, P401, S403):
Forward: 5′- TTACTGCCTCCTGGTTACTTTCGGGGTCCGCCATTT TCTCCTGTC-3′
Reverse
5′- GACAGGAGAAAATGGCGGACCCCGAAAGTAACCAGGAGGCAG TAA-3′

TRIP12 WT was cloned into pCMV-3xF-turboID via Gibson assembly. Generation of the catalytically inactive TRIP12 was performed using a PCR-based site-directed mutagenesis kit, QuikChange Lightning (Agilent).

3xF TID TRIP12 EcoRI Fwd
5′ ggtctgccgaaaagGAATTCatgtccaaccggcctaat 3′
3xF TID TRIP12 KpnI Rev
5′ CCTCTAGAGTCGACTGGTACCttaggaaagatggaacga 3′
Catalytic Cysteine C2007A Mutagenesis Primers
Forward: 5′ atgacttcttgccctctgtaatgactgctgtgaactatcttaagttg 3′
Reverse: 5′ caacttaagatagttcacagcagtcattacagagggcaagaagtcat 3′

Cell lines and transfections

Human cell cultures were maintained at 37 °C in a humidified 5% CO_2 environment.

HEK293T cell lines were purchased from the American Type Culture Collection (ATCC CRL-3216). HEK293STF cells were a gift from

https://doi.org/10.1038/s41467-025-60535-5

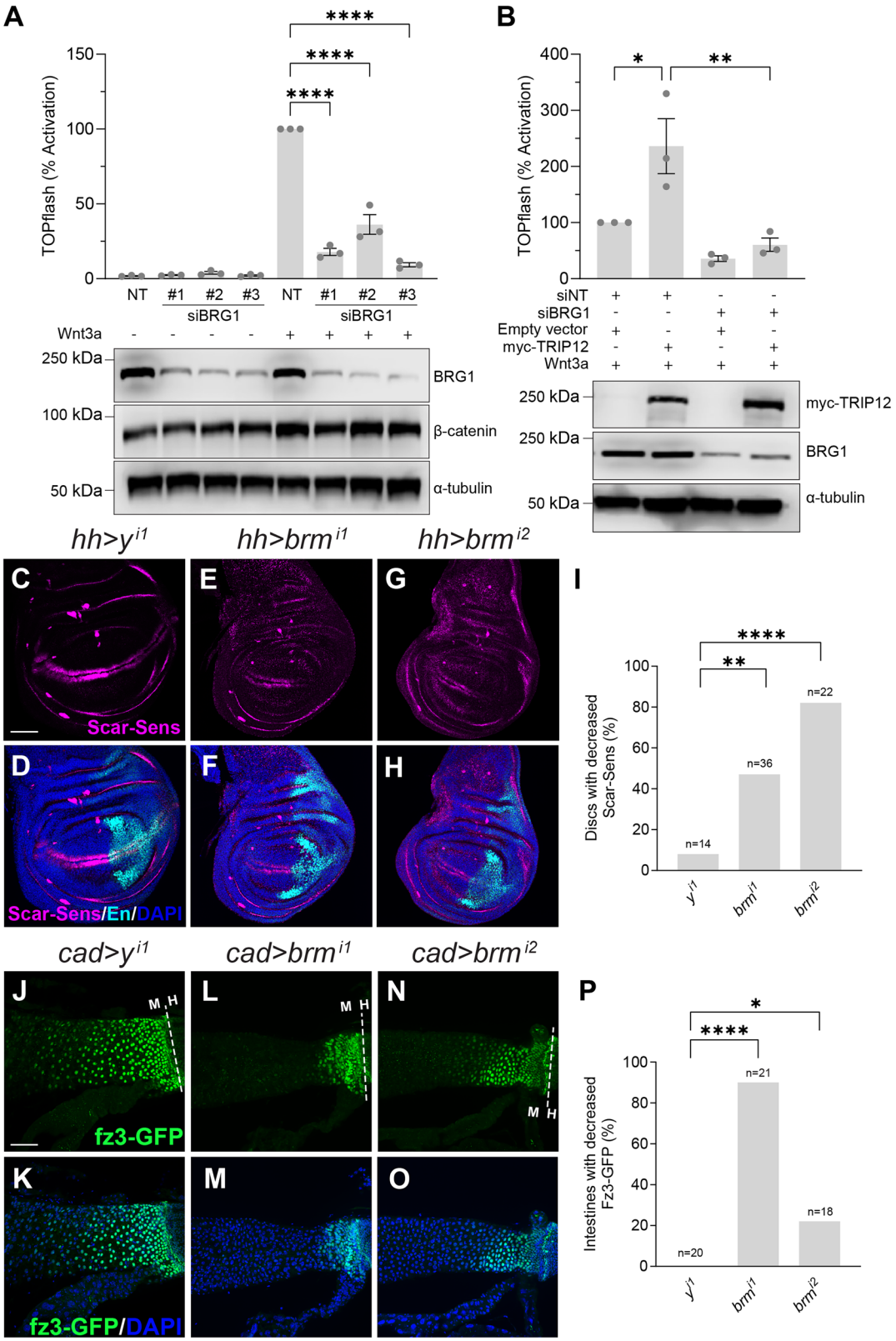

Jeremy Nathans (Johns Hopkins University). HEK293 cell lines were cultured in DMEM with 10% fetal bovine serum (ThermoFisher Scientific) and 1% penicillin–streptomycin 10,000 U/mL (ThermoFisher Scientific). DNA transfections were performed using $CaCl_2$ as follows: An individual well of a 12-well plate was transfected with 1 μg of DNA mixed with 6.1 μl of 2X $CaCl_2$ and sterile water to a final volume of 50 μl that was mixed with a tube containing 50 μl of 2x HBS (280 mM NaCl, 10 mM KCl, 1.5 mM Na_2HPO_4-$2H_2O$, 12 mM Dextrose (D-Glucose), and 50 mM HEPES), by bubbling air, and added dropwise to the cells. siRNA transfections were performed with Dharmafect-1. The following siRNAs were used:

NT siRNA: 5′ – CCUACGCCACCAAUUUGGUU-3′
TRIP12 siRNA#1: 5′ – UGGCAGACCCUGAAAGCAAUU-3′
TRIP12 siRNA#2: 5′ – GAACACAGAUGGUGCGAUAUU-3′

Fig. 6 | BRG1 promotes Wnt/Wingless signaling. A HEK293STF cells transfected with nontargeting (siNT) control or three independent BRG1 siRNAs (siBRG1 #1, #2, and #3), incubated in the absence or presence of recombinant Wnt3a. TOPflash reporter quantified, and cell extracts immunoblotted for BRG1 and β-catenin. For **A** and **B**, graphs show mean ± SEM of TOPflash normalized to cell number and NT control. Significance assessed using one-way ANOVA with Dunnett's test. All TOPflash results and immunoblots represent at least three independent experiments. $n = 3$ wells of cells per treatment group per experiment. α-tubulin is a loading control. p-values for siNT + Wnt3a versus siBRG1#1 + Wnt3a, siBRG1#2 + Wnt3a, and siBRG1#3 + Wnt3a are all <0.0001. **B** HEK293STF cells transfected with indicated expression constructs and incubated in the presence of recombinant Wnt3a. TOPflash reporter activity quantified, and cell extracts immunoblotted for Myc-TRIP12 and BRG1. p-value for siNT versus siNT + myc-TRIP12 is 0.0218 and for siNT + myc-TRIP12 versus siBRG1 + myc-TRIP12 is 0.0052. **C**–**H** RNAi constructs targeting *yellow (y)* control or *brahma* (*brm)* expressed in posterior compartment (marked by Engrailed (En, cyan)) of third instar larval wing discs using *hedgehog (hh)-Gal4*. *Scarlet-Senseless* (Scar-Sens, magenta) is a Wingless target gene reporter. **C**, **D** *hh-Gal4*-driven expression of *y* RNAi. Minimal loss of Scar-Sens was observed. **E**–**H** *hh-Gal4*-driven expression of independent RNAi targeting *brm* resulted in decreased Scar-Sens in the posterior compartment. Dorsal, top, and posterior, right. **I** Quantification is the percentage of discs with decreased Scar-Sens. *N* is number of wing discs analyzed. **J**–**O** RNAi constructs targeting *y* control or *brm* in posterior midgut using *cad-Gal4*. *frizzled3-GFP* (*fz3-GFP*, green) is a Wingless target gene reporter. **J**, **K** *cad-Gal4*-driven expression of *y* control RNAi. No *fz3-GFP* reduction was observed. **L**–**O** *cad-Gal4*-driven expression of *brm* RNAi resulted in partial loss of *fz3-GFP*. **P** Quantification shown as percentage of intestines with decreased *fz3-GFP*. *N* is the number of adult intestines analyzed. DAPI (blue) marks nuclei. Scale bar (**C**–**H**, **J**–**O**): 50 µm. Statistical significance (**I**, **P**) was analyzed by Fisher's exact test (two-sided). p-values for **I** are 0.0090 and <0.0001. p-values for **P** are <0.0001 and 0.0415. *$p < 0.05$, **$p < 0.01$, ****$p < 0.0001$. Source data are provided.

hAXIN1 siRNA#1: 5′-GCGUGGAGCCUCAGAAGUUUU-3′
hAXIN1 siRNA#2: 5′-CCGAGGAGAAGCUGGAGGAUU-3′
BRG1 siRNA#1: 5′ – GCUCAGAAGAAGAGGAAGAUU-3′
BRG1 siRNA#2: 5′ – CCAAGGAUUUCAAGGAAUAUU-3′
BRG1 siRNA#3: 5′ – GGCAGAAGCACCAGGAAUAUU-3′
APC siRNA#1: 5′ - CUGAAGAUGAUGAAAGUAAUU-3′
APC siRNA#2: 5′ – UGAUAAUGAUGGAGAACUAUU-3′

Axin and APC siRNA knockdowns were performed by pooling hAXIN1 or APC siRNA#1 and siRNA#2. Similarly, unless otherwise stated, TRIP12 siRNA knockdowns were performed by pooling TRIP12 siRNA#1 and siRNA#2, and BRG1 siRNA knockdowns were performed by pooling BRG1 siRNA#1 and siRNA#3.

Immunoblotting and immunoprecipitation

Cells were lysed in non-denaturing lysis buffer (NDLB) (50 mM Tris-Cl (pH 7.4), 300 mM NaCl, 5 mM EDTA, 1% Triton X-100) with 1 mM PMSF. For co-immunoprecipitations, PhosStop phosphatase inhibitor cocktail tablets (Roche) were added to NDLB with 1 mM PMSF. Cells were lysed and diluted to 1 mg/ml with lysis buffer. Lysates were incubated with antibody at 4 °C with rotation overnight, followed by the addition of protein A/G magnetic beads (Santa Cruz) for 2 h. Beads were washed five times with NDLB, and bound proteins were eluted with 6x sample buffer and analyzed by immunoblotting. HEK-293T cells stably expressing 3xFLAG-TRIP12 were lysed in low salt lysis buffer supplemented with complete protease and phosphatase inhibitors. Lysates were sonicated prior to centrifugation at 15,000 × *g* 4 °C for 15 min. Protein lysates were incubated rotating with pre-equilibrated Anti-FLAG M2 Affinity gel beads for 3 h at 4 °C. Beads were subsequently washed three times in lysis buffer, and complexes were eluted using FLAG peptide and analyzed via quantitative MS as described in the label-free LC-MS/MS analysis section. All experiments were done in triplicate.

Antibodies for immunoblotting and immunoprecipitation

Antibodies used were Rabbit anti-TRIP12 (1:5000, A301-814A) from Bethyl, Mouse anti-BRG1 (1:1000, G-7), Rabbit anti-APC (1:1000, sc-7930) and Mouse IgG (1:250, sc-2025) from Santa Cruz, Rabbit anti-Axin (1:1000, C76H11), Rabbit anti-BRG1 (1:1000, D1Q7F), HA-tag (1:1000, C29F4) Rabbit mAb and Rabbit anti-Histone H3 (1:25,000) from CST, Rabbit anti-DYKDDDDK (FLAG) (1:1000, 20543-1-AP) from Proteintech, Mouse anti-V5 (1:1000, SV5-Pk1) from Bio-Rad, Mouse anti-GAPDH (1:500) from Developmental Studies Hybridoma Bank (DSHB), Goat anti-mouse IgG H + L-HRP (1:5000, W4021) and Goat anti-rabbit IgG H + L-HRP (1:5000, W4011) from Promega, Mouse anti-Vinculin (1:1000, V9131) and Mouse anti-FLAG M2 (1:1000, F3165) from Sigma, Anti-MUC2 antibody (1:500,ab272692) from Abcam, Mouse anti-beta-catenin (1:1000), Mouse anti-Tubulin (1:5000), Mouse anti-Myc (1:1000), Mouse anti-FLAG (1:500), Mouse anti-MBP (1:1000) and Mouse anti-HA (1:1000) from Vanderbilt Antibody and Protein Research Core, IRDye 800CW Goat anti-Rabbit IgG (H + L) (1:10,000, 926-32211) and IRDye 800CW Donkey anti-Mouse IgG (H + L) (1:10,000, 926-32212) from LICOR. Alexa Fluor 790 IgG Fraction Monoclonal Mouse Anti-Rabbit IgG, light chain specific (1:10,000) from Jackson ImmunoResearch.

Ubiquitylation assays

In vitro ubiquitylation assays were performed in 30 µl reactions using the Ubiquitylation Assay Kit (Abcam) and the following: 1.5 µg UbcH5a (R&D Systems), 10 µg of GST-TRIP12-HECT (NovoPro), and 200 ng of recombinant BRG1 (ProteinOne #P1041-02). FLAG-BRG1 was prepared by transfection of HEK293FT cells with FLAG-BRG1. 2 mg at a concentration of 2 mg/ml was taken for immunoprecipitation. FLAG-BRG1 was pulled down with an anti-FLAG antibody, beads were washed five times with NDLB, and BRG1 was eluted with FLAG peptide (Millipore Sigma) (500 µg/ml) in NDLB at 4 °C for 1 h on shaker. The eluate was used as a substrate. Recombinant MBP was used as a negative control. Reactions were carried out at 37 °C for 90 min and were terminated by the addition of sample buffer. Reaction products were resolved by SDS-PAGE and visualized by immunoblotting. For the ubiquitin mutant in vitro ubiquitylation assays, 100 ng of recombinant BRG1 (ProteinOne #P1041-02) and 1 µg of ubiquitin (Single Lysine Ubiquitin Explorer Panel, LifeSensors S1210) were used. For the tandem ubiquitin-binding entity (TUBE) assay[81] cells were treated with 20 ng/ml of recombinant Wnt3a overnight. Cells were treated with 10 mM of the proteasome inhibitor MG132 (Sigma-Aldrich) or dimethyl sulfoxide for 4 h. Cells were lysed in NDLB with 1 mM PMSF and PhosStop phosphatase inhibitor tablets (Roche) and diluted to 1 mg/ml with lysis buffer. Lysates were incubated with 50 µg of MBP-TUBE protein at 4 °C with rotation overnight, followed by the addition of amylose resin (NEB) for 2 h. The resin was washed five times with 0.1% TBS-Tween, and bound proteins were eluted with 6x sample buffer and analyzed by immunoblotting.

Immunofluorescence and proximity ligation assay

For immunofluorescence studies and Proximity Ligation Assays, RPE cells were used as they better adhere to coverslips than HEK293T cells. For immunofluorescence studies, RPE cells were seeded on coverslips in 6-well plates and allowed to adhere overnight. Cells were treated with 20 ng/ml of recombinant Wnt3a overnight. Cells were fixed with 3.7% PFA and permeabilized in 0.5% TBS-Triton and blocked with Abdil (0.1% Triton, 1% Sodium Azide, 2% BSA, TBS) for 1 h at room temperature. Cells were stained with primary antibodies for TRIP12 (Bethyl, #A301-814A, 1:500), β-catenin (Vanderbilt Antibody and Protein Research Core, 1:500), BRG1 (Santa Cruz G-7, 1:500), and TLE3 (Santa Cruz D-10, 1:500) at 4 °C overnight. Washes were performed two times with 0.1% TBS-Triton followed by incubation with anti-rabbit Alexa Fluor 488 (ThermoFisher, A-11008, 1:1000) and anti-mouse Cyanine3 (ThermoFisher, A10521, 1:1000) for 2 h in the dark at room temperature. Cells were stained with Hoescht for 15 min, washed three

https://doi.org/10.1038/s41467-025-60535-5

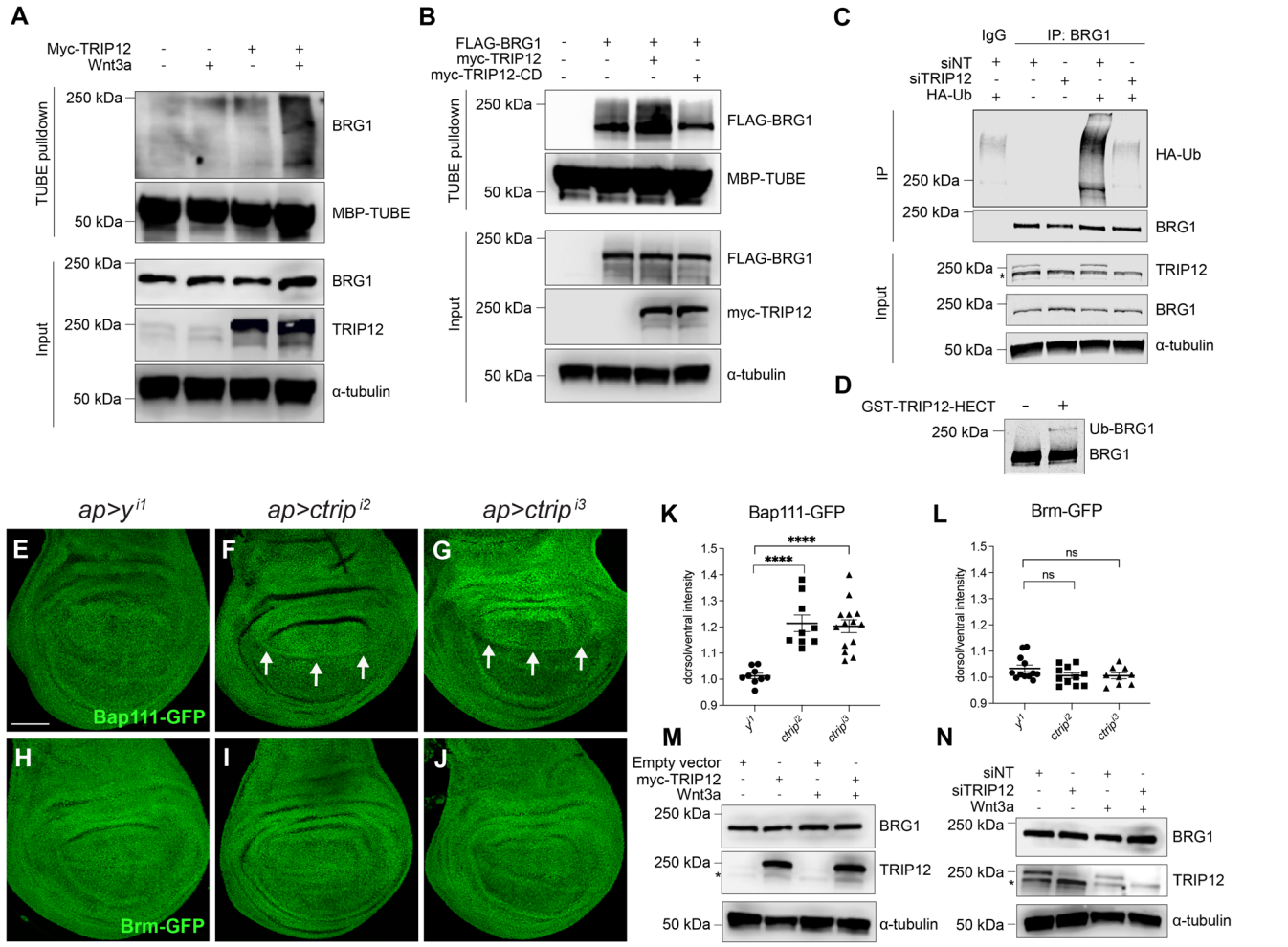

Fig. 7 | TRIP12 ubiquitylates BRG1 but does not affect its stability. **A** HEK293FT cells were transfected with Myc-TRIP12 with or without Wnt3a and MG132 treatment. In **A** and **B**, ubiquitylated proteins were pulled down with MBP-TUBE. BRG1 and TRIP12 were detected by immunoblotting. MBP-TUBE and α-tubulin are loading controls. **B** HEK293FT cells transfected with control vector, Myc-TRIP12 wild-type (TRIP12) or Myc-TRIP12 catalytic dead (TRIP12-CD) and FLAG-BRG1 and treated with Wnt3a and MG132. **C** HEK293FT cells were transfected with nontargeting (siNT) or two pooled TRIP12 siRNAs and control vector or HA-Ubiquitin (HA-Ub). Cells treated with Wnt3a and MG132 and extracts immunoprecipitated with BRG1 antibody or immunoglobulin G (IgG). Ubiquitylated BRG1 detected with HA antibody. **D** Recombinant BRG1 incubated with GST-TRIP12-HECT domain. Ubiquitylated BRG1 was detected by immunoblotting. **E**–**L** *yellow (y)* control or *ctrip* RNAi expressed in the dorsal compartment of larval wing discs using *apterous (ap)-Gal4*. **E**, **H**, **K**, **L** *ap-Gal4*-driven expression of *y* RNAi control. No change observed in Bap111-GFP (green) or Brm-GFP (green) levels. **F**, **G**, **K** *ap-Gal4*-driven expression of *ctrip* RNAi increased Bap111-GFP (green) levels in the dorsal compartment. **I**, **J**, **L** *ap-Gal4*-driven expression of *ctrip* RNAi in the dorsal compartment results in no change in Brm-GFP levels (green). Arrows denote the dorsal-ventral boundary. **K**, **L** Quantification of GFP mean intensity as dorsal-ventral ratio. Bap111 level increased in the dorsal compartment upon Ctrip knockdown and quantified **K**. Graphs show mean ± SEM, $n = 9, 9, 14$ in **K**, $n = 12, 11, 9$ in **L**. *N* is the number of wing discs analyzed. Significance assessed using one-way ANOVA with Dunnett's test, comparing genotypes to control (y^{i1}). *p*-values for **K** are both <0.0001. *p*-values for **L** are 0.1749 and 0.1986. Scale bar (**E**–**J**): 50 µm. Dorsal, top; posterior, right. **M** HEK293FT cells transfected with empty vector or Myc-TRIP12, treated with recombinant Wnt3a, and immunoblotted for TRIP12 and BRG1. *indicates nonspecific band in **M** and **N**. **N** HEK293FT cells transfected with nontargeting (siNT) control or TRIP12 siRNAs, treated with recombinant Wnt3a. Lysates were immunoblotted for endogenous TRIP12 and BRG1. α-tubulin is a loading control. All immunoblots represent at least three independent experiments. $^{****}p < 0.0001$, $p \geq 0.05$ is not significant (ns). Source data provided.

times with 0.1% TBS-Triton, and mounted using Prolong Gold. Images were acquired using a Nikon sCMOS camera mounted on a Nikon Eclipse 80i fluorescence microscope with a 40× objective. For Proximity Ligation Assays, RPE cells were seeded on coated coverslips (Fisher Scientific, #08-774-383). Cells were treated with 50 ng/ml of recombinant Wnt3a for 4 h. Cells were washed three times with PBS, fixed with 3.7% PFA, washed three times with PBS, permeabilized with 0.5% TBS-Triton, washed three times with 0.1% TBS-Triton, and coverslips were moved to a slide moisture chamber (Fisher Scientific, #23-769-522). Duolink In Situ Red Starter Kit Mouse/Rabbit (Millipore Sigma, #DUO92101) was used according to the manufacturer's protocol. Cells were stained with primary antibodies for TRIP12 (Bethyl, #A301-814A, 1:500), BRG1 (Santa Cruz G-7, 1:500) and TLE3 (Santa Cruz D-10, 1:500) overnight at 4 °C. Coverslips were mounted with Prolong Gold with DAPI (ThermoFisher, P36931). Images were acquired using a Nikon sCMOS camera mounted on a Nikon Eclipse 80i fluorescence microscope with a 40× objective. Intensities were measured using ImageJ (National Institutes of Health).

Reporter and HiBiT assays

For cell-based TOPFlash and HiBiT assays, cells were plated and transfected with DNA or siRNA, as described above. Recombinant murine Wnt3a (TIME Bioscience) was added to HEK293STF cells 24 h after transfection. 24 h after Wnt3a treatment, cells were lysed with 1x Passive Lysis Buffer (Promega), and luciferase activity was measured with Steady Glo (Promega) for TOPflash assays or with the Nano-Glo

https://doi.org/10.1038/s41467-025-60535-5

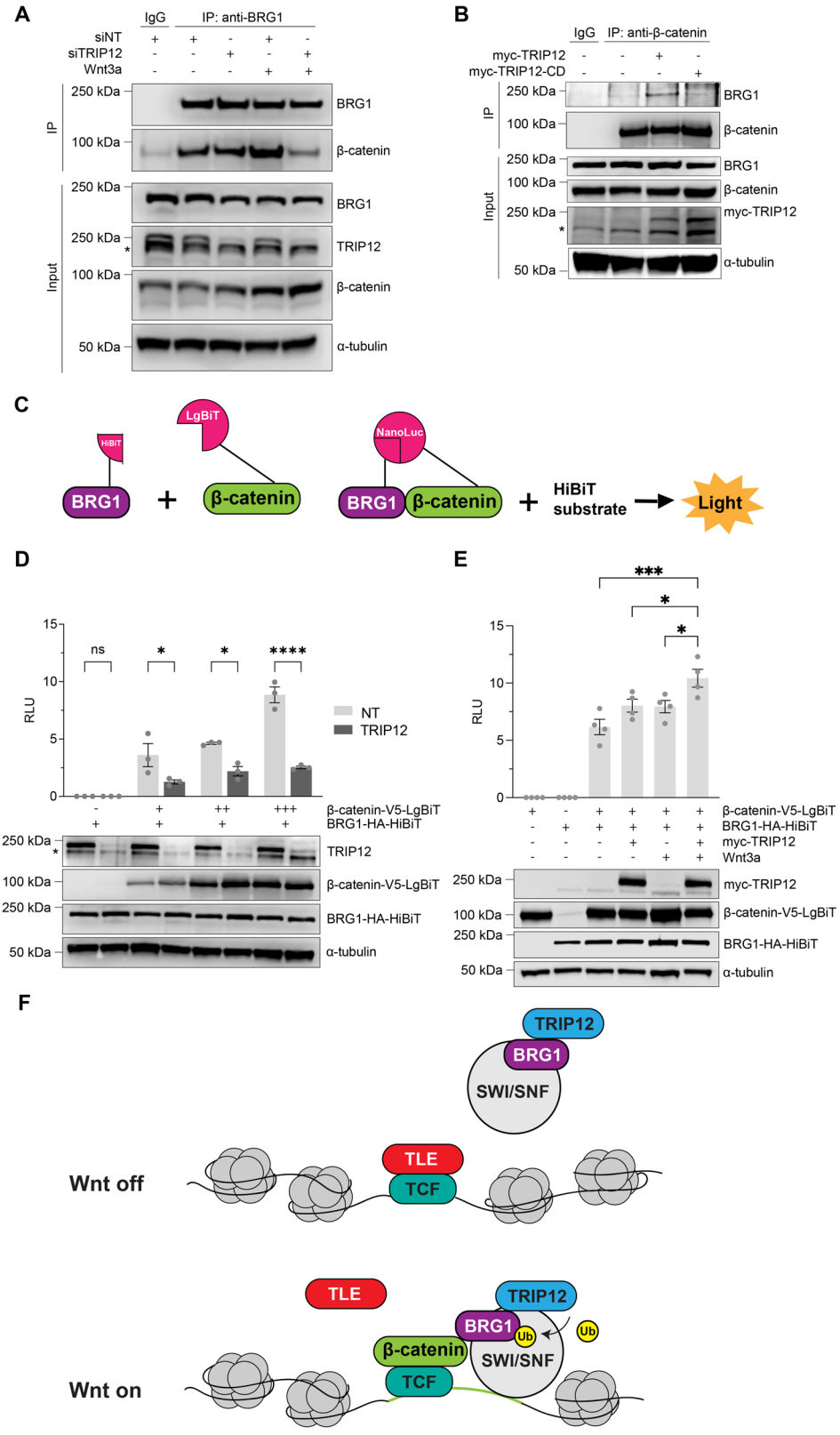

HiBiT lytic substrate (Promega) for HiBiT assays. Luciferase activity was normalized to viable cell numbers with CellTiter-Glo (Promega). All assays were performed in triplicate.

RNA isolation and RT-qPCR

HEK293T cells were incubated with Wnt3a for 8 h and total RNA was isolated using RNAeasy RNA extraction kit (Qiagen). RNA was reverse transcribed to cDNA using the High-Capacity cDNA Reverse Transcription kit (Applied Biosystems). qPCR assays were performed in quadruplicate using TaqMan FAST Advanced Real-time PCR Master Mix (Applied Biosystems) and analyzed on a CFX96 Real-Time PCR system (Bio-Rad). Predesigned and validated TaqMan probes (Life Technologies) were used as follows: *GUSB* (Hs00939627_m1), *SP5* (Hs01370227_mH), *AXIN2* (Hs00610344_m1),

Fig. 8 | TRIP12 promotes the interaction of BRG1 with β-catenin. **A** HEK293FT cells were transfected with nontargeting (siNT) control or two pooled TRIP12 siRNAs and incubated in the presence or absence of Wnt3a. Endogenous BRG1 was immunoprecipitated with a BRG1 antibody. IgG was used as a negative control. Coimmunoprecipitated, endogenous β-catenin was detected by immunoblotting. *indicates a nonspecific band. **B** HEK293FT cells were transfected with wild-type or catalytic dead TRIP12 as indicated. Endogenous β-catenin was immunoprecipitated with a β-catenin antibody. IgG was used as a negative control. Coimmunoprecipitated, endogenous BRG1 was detected by immunoblotting. Immunoblots are representative of at least three independent experiments. α-tubulin is a loading control. *indicates a nonspecific band. **C** HiBiT-tagged BRG1 was co-overexpressed with LgBiT-tagged β-catenin. When the two proteins are in close proximity, the HiBiT and LgBiT proteins interact and form a functional NanoBit luciferase enzyme. Addition of the HiBiT substrate results in an enzymatic reaction that produces a light signal, which was used as a readout for the interaction between BRG1 and β-catenin. HEK293FT cells were transfected as indicated and TRIP12 was knocked down (**D**) or overexpressed (**E**). Cells were treated with or without Wnt3a as indicated and luminescence was quantified as relative light units (RLU). Cell extracts were immunoblotted for TRIP12, β-catenin-V5-LgBiT, and BRG1-HA-HiBiT. *indicates a nonspecific band. α-tubulin is a loading control. Graphs show mean ± SEM of luminescence normalized to cell number. Significance was assessed using the one-way ANOVA with Tukey's test. *p*-value for NT versus TRIP12 is >0.9999 (–), 0.0401 (+), 0.0297 (++), and <0.0001 (+++). *p*-value for myc-TRIP12 + Wnt3a versus control is 0.0002, versus myc-TRIP12 is 0.0473, and versus control + Wnt3a is 0.0369. All HiBiT results and immunoblots are representative of at least three independent experiments. $n = 3–4$ wells of cells per treatment group per experiment. **F** Upon Wnt pathway activation, TRIP12 ubiquitylates BRG1 and promotes BRG1 association with β-catenin. $^{*}p < 0.05$, $^{***}p < 0.001$, $^{****}p < 0.0001$, $p \geq 0.05$ is not significant (ns). Source data are provided in Source Data file.

and *DKK1* (Hs00183740_m1). All qPCR amplifications were performed in biological and technical triplicate.

TurboID labeling of proximal interactors

HEK293T cells stably expressing TRIP12 were treated with 50 μM biotin for 1 h. Cells were lysed and homogenized in RIPA buffer (50 mM Tris pH 7.5, 500 mM NaCl, 0.1% Triton X-100, 1% NP-40, 0.1% SDS) supplemented with protease (need brand) and phosphatase inhibitors (100 mM NaF, 100 mM NaMolybdate, 100 mM beta-glycerophosphate). Protein lysates were incubated rotating with pre-equilibrated StrepTactin beads for 4 h at 4 °C. Beads were subsequently washed three times in RIPA buffer, and biotinylated proteins were eluted using biotin elution buffer (50 mM Tris pH8, 500 mM NaCl, 1 mM biotin). Eluates were processed using single-pot solid-phase-enhanced sample preparation (SP3) prior to trypsin digest overnight and subsequently analyzed via label-free LC-MS/MS analysis[82].

Label-free LC-MS/MS analysis

FLAG IP-MS experiments were analyzed on a Q-Exactive Plus quadrupole Orbitrap mass spectrometer (Thermo Scientific) equipped with an Easy-nLC 1000 (Thermo Scientific) and nanospray source (Thermo Scientific). Peptides were resuspended in 5% methanol/1% formic acid and loaded onto analytical resolving column (35 cm length, 100 μm inner diameter, ReproSil, C18 AQ 3 μm 120 Å pore (Dr. Maisch, Ammerbuch, Germany)) pulled in-house (Sutter P-2000, Sutter Instruments, San Francisco, CA) with a 45 min gradient of 5–30% LC-MS buffer B (LC-MS buffer A: 0.0625% formic acid, 3% ACN; LC-MS buffer B: 0.0625% formic acid, 95% ACN).

TurboID-based biotinylation experiments and BRG1 IP-MS experiments were analyzed on an Orbitrap Fusion Lumos mass spectrometer (Thermo Scientific) equipped with an Easy-nLC 1200 (Thermo Scientific). Peptides were resuspended in 5% methanol/1% formic acid and loaded onto a column (45 cm length, 100 μm inner diameter, ReproSil, C18 AQ 1.8 μm 120 Å pore) pulled in-house across a 2 h gradient from 3% acetonitrile/0.0625% formic acid to 37% acetonitrile/0.0625% formic acid.

Quantification of all LC-MS/MS spectra was performed using MassChroQ and the iBAQ method[83,84]. Data were filtered to a <1% FDR at the peptide level, and proteins that were fully quantified in all experimental replicates were kept and normalized to TRIP12 iBAQ intensities. Imputation for missing values in control replicates was performed matrix-wide in Perseus, and keratins were filtered out from the final dataset. Volcano plots were generated using ggplot2 in RStudio.

Over-representation analysis of enriched gene ontology terms

358 commonly identified proteins from both proximity labeling and FLAG AP-MS approaches were used in performing ORA via WebGestalt using the GO biological process against a background of human protein-encoding genes[85]. Enriched gene sets were post-processed using affinity propagation clustering methods to reduce redundancy[86].

TCGA data analysis

To evaluate TRIP12 mRNA expression in The Cancer Genome Atlas, we utilized the cBioPortal interactive web-based application[87]. Pancreatic adenocarcinoma patients from the TCGA PanCancer Atlas cohort (Pancreatic Adenocarcinoma (TCGA, PanCancer Atlas)) were selected for analysis. Of the 184 patients in this cohort, 177 patients had mRNA expression data. These 177 patients were split into two groups using a 50th percentile cutoff of TRIP12 mRNA expression z-scores relative to all samples (log RNA Seq V2 RSEM). For each group, a survival curve was plotted showing the probability of overall survival over time (months). Significance was determined using the log-rank test comparing the two groups (*p*-value = 0.0366).

Organoid cultures

The isolation and culture of APC^{min} mouse intestinal organoids were performed as previously described[88]. APC^{min} organoids were digested with Gentle Cell Dissociation Reagent (Stemcell Technologies) for 10 min at RT and sheared once with a 25G needle. Dissociated organoids were added to a lentiviral mixture containing lentiviral particles (MOI = 10), 8 μg/ml polybrene, and 10 μm Y27632 (Stemcell Technologies) in 25% L-WRN-conditioned media. The mixture was then spinoculated at 600 × g for 2 h using a tabletop centrifuge at RT, followed by incubation at 37 °C for 4 h. Infected organoids were resuspended in Matrigel (Stemcell Technologies), plated at 10,000/well in a 48-well plate, and overlaid with culture media. Organoids were imaged and lysed for immunoblotting after 9 days. Image acquisition was performed with an Olympus IX51 inverted fluorescence microscope using Olympus CellSens software, and organoid size was measured using the Olympus CellSens software. For immunoblotting, organoids were lysed in RIPA buffer (Thermo) supplemented with a Protease/Phosphatase inhibitor cocktail (Thermo). Lysates were boiled in SDS sample buffer for 10 min, followed by SDS-PAGE analysis and immunoblotting. For immunostaining experiments, organoids were grown in 40 μl of matrigel plated into a glass coverslip treated with poly-L-Lysine (Corning, #354085). The growth media was removed, and the organoids were fixed in 4% PFA for 20 min. They were then permeabilized in PBS with 0.1% triton permeabilized for 20 min. After three PBS washes, they were blocked in blocking buffer (PBS with 5% goat serum (Invitrogen, # 31872) for 1 h. Cells were incubated in primary antibody overnight in blocking buffer: mouse anti-Muc (1:200, Invitrogen, MA5-12345) or no primary antibody as a negative control. They were then washed 3 times with PBS. Secondary mouse antibody Cy3 (1:1000, Invitrogen, A10521) was incubated for 1 h followed by PBS washes. Prolong Gold antifade medium with DAPI (Invitrogen, #P36941) was used for mounting. Images were acquired using a Keyence BZ-X800

fluorescence microscope. Images were processed with Photoshop CS5 software (Adobe Systems Inc., San Jose, CA).

Multiplex immunofluorescence of formalin-fixed paraffin-embedded (FFPE) tissue

De-identified normal human intestinal tissue was obtained through an IRB-approved Exempt Study (IRB #231475). Formalin-fixed paraffin-embedded tissue from de-identified subjects was obtained without clinical history or a link back to the original study subject. Unstained slides were collected and used for multiplex immunofluorescence. Normal colon tissue FFPE blocks were cut into 5 μm sections and stored at −20 °C. Tissue sections were thawed overnight at room temperature and heated for 1 h at 60 °C. Tissue sections were deparaffinized with xylene (2 × 15 min), ethanol (100% 2 × 5 min, 95% 1 × 5 min), and water (5 min) and washed with PBS. Slides were heated for 45 min in sodium citrate buffer (pH 6.0) in a rice cooker, followed by 30 min at room temperature for antigen retrieval. Tissues were washed with PBS and blocked for 2 h with 10% goat serum in PBS (blocking buffer). Primary antibodies (BD Transduction Laboratories 610154 mouse anti-β-catenin diluted 1:300; Bethyl Laboratories #A301-814A rabbit anti-TRIP12 diluted 1:100; Santa Cruz G-7 mouse anti-BRG1 diluted 1:100), diluted in blocking buffer, were incubated on tissue sections at 4 °C for 16 h. Tissue sections were washed with 0.05% Tween 20 in PBS. Secondary antibodies (Abcam ab97035 goat anti-mouse Cy3 1:100; Invitrogen A-21245 goat anti-rabbit Alexa fluor 647 1:150) were diluted in blocking buffer containing Hoechst 33342 nuclear stain (1:1000) and incubated on tissue sections at 37 °C for 1 h. Images were acquired using a Nikon Spinning Disc confocal microscope.

Zebrafish injections

Wild-type (NHGRI) or Tg(myl7:GFP) were used for all experiments. Fish were phenotyped at 3 days post-fertilization (dpf). Only phenotypes observed in $n \geq 3$ biological repeats were reported. Embryos from $n \geq 3$ male/female pairs were collected per biological repeat. Data are aggregated from all biological repeats. Embryos with severe and nonspecific edema were excluded from the analysis. For mRNA injections, capped mRNAs were generated using mMessage mMachine (Ambion) according to the manufacturer's instructions. Zygotes (1 cell) were injected (1 ng mRNA in 1 nl) into the single cell. Morpholinos were injected into the yolk (6 ng MO in 3 nl). MOs with the following sequences were purchased from Gene Tools:

Standard Control: 5′–CCTCTTACCTCAGTTACAATTTATA–3′

TRIP12: 5′–GGACATTGGCACCTCTCTCCTGAAG–3′

For zebrafish CRISPRi studies, embryos were injected with combinations of 250 pg dCas9 mRNA and/or 500 pg Alt-R sgRNA in 1 nL into a single cell. The following guides were purchased from Integrated DNA Technologies:

guide #1: 5′–ACCGGCCUAAUUCCAAUCCA–3′

guide #2: 5′–GAGAGGUGCCAAUGUCCAAC–3′

To assess the degree of CRISPRi-mediated transcriptional down-regulation, qRT-PCR of TRIP12 was performed on pools of 10 fish collected at 24 hpf in TRIzol to isolate total RNA. cDNA was generated with the High Capacity cDNA Reverse Transcription Kit (Applied Biosystems) and ran on a QuantStudio 5 (Applied Biosystems) using the following primers:

TRIP12 Set #1:

Forward: 5′–GCCAGTCAGAGAAGATGAAGAG–3′

Reverse: 5′–CGTCCTGTTTCTTGGCATTTC–3′

TRIP12 Set #2:

Forward: 5′–CACCACCTGCAGTACTTCTATC–3′

Reverse: 5′–GTCTGCAGCACTCCATTAGT–3′

Embryos analyzed for qRT-PCR were from $n = 3$ clutches of embryos from $n \geq 2$ breeding pairs.

Microscopy of zebrafish embryos

Fish were fixed for 2 h at room temperature with 4% PFA at 3 dpf and stored at 4 °C until imaging. Eyes and spine defects were imaged in glycerol and pericardial edema and cardiac malformations were imaged in methylcellulose. Bright field images were obtained using a Stemi 2000-CS microscope (Zeiss, Oberkochen, Germany) with an Olympus DP72 camera. Images were analyzed in Fiji and Photoshop.

Statistical analysis

For the cultured cell experiments, graphs were made using Prism 9 (GraphPad Software, Inc.), and statistical analysis was performed using the one-way ANOVA with a follow-up Tukey's or Dunnett's test. A value of $p < 0.05$ was considered statistically significant. For zebrafish studies, data were analyzed with PRISM 9 software. Statistical analyses were performed in R v3.1.0. Statistical analysis was performed using Fisher's exact test and multiple t-tests (two-tailed, equal variance). Post hoc analysis of Fisher's exact test and multiple t-tests tests were by Bonferroni correction. Sample sizes (n) are indicated as n = number of samples, with the number of the observed phenotype over the total sample number. For *Drosophila* studies, quantification of progenitor cells in the adult midgut, *esg> GFP* positive cells in a field of 60× objective lens in the R5A region were counted. Quantification of Bap111-GFP and Brm-GFP signals was performed with ImageJ, mean intensity of GFP was measured in the dorsal and ventral compartments. Statistical analysis was performed using the one-way ANOVA with a follow-up Dunnett's test and Fisher's exact test (two-sided). For organoid studies, data were analyzed with Prism 9 and statistical analysis was performed using one or two-tailed Student's t test or a chi-square test. A minimum of three independent replicates were performed for each experiment. Statistical tests were performed using Prism 9 software. $^{*}p < 0.05$, $^{**}p < 0.01$, $^{***}p < 0.001$, $^{****}p < 0.0001$.

Reporting summary

Further information on research design is available in the Nature Portfolio Reporting Summary linked to this article.

Data availability

All data supporting the findings of this study are available within the published article and the Supplementary Information files. Requests for reagents should be directed to the lead contacts: Ethan Lee (ethan.lee@vanderbilt.edu) and Yashi Ahmed (yashi.ahmed@dartmouth.edu). Raw data and original gel images are included in the Source Data file, which is provided with this paper. Proteomic data were deposited in ProteomeXchange (PXD048292) and MassIVE (MSV000093784). Source data are provided with this paper.

References

1. Horn, P. J. & Peterson, C. L. Heterochromatin assembly: a new twist on an old model. *Chromosome Res.* **14**, 83–94 (2006).
2. Peterson, C. L. & Herskowitz, I. Characterization of the yeast SWI1, SWI2, and SWI3 genes, which encode a global activator of transcription. *Cell* **68**, 573–583 (1992).
3. Kwon, H., Imbalzano, A. N., Khavari, P. A., Kingston, R. E. & Green, M. R. Nucleosome disruption and enhancement of activator binding by a human SW1/SNF complex. *Nature* **370**, 477–481 (1994).
4. Rim, E. Y., Clevers, H. & Nusse, R. The Wnt pathway: from signaling mechanisms to synthetic modulators. *Annu. Rev. Biochem.* **91**, 571–598 (2022).
5. Saito-Diaz, K. et al. The way Wnt works: components and mechanism. *Growth Factors* **31**, 1–31 (2013).
6. Logan, C. Y. & Nusse, R. The Wnt signaling pathway in development and disease. *Annu. Rev. Cell Dev. Biol.* **20**, 781–810 (2004).
7. Bugter, J. M., Fenderico, N. & Maurice, M. M. Mutations and mechanisms of Wnt pathway tumour suppressors in cancer. *Nat. Rev. Cancer* **21**, 5–21 (2021).

8. Zhong, Z. & Virshup, D. M. Wnt signaling and drug resistance in cancer. *Mol. Pharm.* **97**, 72–89 (2020).
9. Anthony, C. C., Robbins, D. J., Ahmed, Y. & Lee, E. Nuclear regulation of Wnt/β-catenin signaling: it's a complex situation. *Genes* **11**, 886 (2020).
10. Cavallo, R. A. et al. Drosophila Tcf and Groucho interact to repress Wingless signalling activity. *Nature* **395**, 604–608 (1998).
11. Fiedler, M. et al. An ancient Pygo-dependent Wnt enhanceosome integrated by Chip/LDB-SSDP. *eLife* **4**, e09073 (2015).
12. van Es, J. H., Barker, N. & Clevers, H. You Wnt some, you lose some: oncogenes in the Wnt signaling pathway. *Curr. Opin. Genet. Dev.* **13**, 28–33 (2003).
13. Barker, N. et al. The chromatin remodelling factor Brg-1 interacts with beta-catenin to promote target gene activation. *EMBO J.* **20**, 4935–4943 (2001).
14. Belenkaya, T. Y. et al. Pygopus encodes a nuclear protein essential for Wingless/Wnt signaling. *Development* **129**, 4089–4101 (2002).
15. Brack, A. S. et al. BCL9 is an essential component of canonical Wnt signaling that mediates the differentiation of myogenic progenitors during muscle regeneration. *Dev. Biol.* **335**, 93–105 (2009).
16. Hecht, A. The p300/CBP acetyltransferases function as transcriptional coactivators of beta-catenin in vertebrates. *EMBO J.* **19**, 1839–1850 (2000).
17. Flack, J. E., Mieszczanek, J., Novcic, N. & Bienz, M. Wnt-dependent inactivation of the Groucho/TLE Co-repressor by the HECT E3 Ubiquitin Ligase Hyd/UBR5. *Mol. Cell* **67**, 181–193.e185 (2017).
18. Hanson, A. J. et al. XIAP Monoubiquitylates Groucho/TLE to promote canonical Wnt signaling. *Mol. Cell* **45**, 619–628 (2012).
19. Kassel, S. et al. USP47 deubiquitylates Groucho/TLE to promote Wnt-β-catenin signaling. *Sci. Signal* **16**, eabn8372 (2023).
20. Lebensohn, A. M. et al. Comparative genetic screens in human cells reveal new regulatory mechanisms in WNT signaling. *eLife* **5**, e21459 (2016).
21. Xu, Q. et al. Vascular development in the retina and inner ear: control by Norrin and Frizzled-4, a high-affinity ligand-receptor pair. *Cell* **116**, 883–895 (2004).
22. Thorne, C. A. et al. Small-molecule inhibition of Wnt signaling through activation of casein kinase 1α. *Nat. Chem. Biol.* **6**, 829–836 (2010).
23. Nishiya, N. et al. A zebrafish chemical suppressor screening identifies small molecule inhibitors of the Wnt/beta-catenin pathway. *Chem. Biol.* **21**, 530–540 (2014).
24. van de Water, S. et al. Ectopic Wnt signal determines the eyeless phenotype of zebrafish masterblind mutant. *Development* **128**, 3877–3888 (2001).
25. Xing, Y. Y. et al. Mutational analysis of dishevelled genes in zebrafish reveals distinct functions in embryonic patterning and gastrulation cell movements. *PLoS Genet.* **14**, e1007551 (2018).
26. Langdon, Y. G. & Mullins, M. C. Maternal and zygotic control of zebrafish dorsoventral axial patterning. *Annu. Rev. Genet.* **45**, 357–377 (2011).
27. Shimizu, T., Bae, Y. K., Muraoka, O. & Hibi, M. Interaction of Wnt and caudal-related genes in zebrafish posterior body formation. *Dev. Biol.* **279**, 125–141 (2005).
28. Dohn, T. E. & Waxman, J. S. Distinct phases of Wnt/beta-catenin signaling direct cardiomyocyte formation in zebrafish. *Dev. Biol.* **361**, 364–376 (2012).
29. Cantu, C. et al. Mutations in Bcl9 and Pygo genes cause congenital heart defects by tissue-specific perturbation of Wnt/beta-catenin signaling. *Genes Dev.* **32**, 1443–1458 (2018).
30. Ueno, S. et al. Biphasic role for Wnt/beta-catenin signaling in cardiac specification in zebrafish and embryonic stem cells. *Proc. Natl. Acad. Sci. USA* **104**, 9685–9690 (2007).
31. Lamaze, A. et al. The E3 ubiquitin ligase CTRIP controls CLOCK levels and PERIOD oscillations in Drosophila. *EMBO Rep.* **12**, 549–557 (2011).
32. Brunet, M., Vargas, C., Larrieu, D., Torrisani, J. & Dufresne, M. E3 ubiquitin ligase TRIP12: regulation, structure, and physiopathological functions. *Int. J. Mol. Sci.* **21**, 8515 (2020).
33. Zecca, M., Basler, K. & Struhl, G. Direct and long-range action of a Wingless morphogen gradient. *Cell* **87**, 833–844 (1996).
34. Neumann, C. J. & Cohen, S. M. Long-range action of Wingless organizes the dorsal-ventral axis of the Drosophila wing. *Development* **124**, 871–880 (1997).
35. Nolo, R., Abbott, L. A. & Bellen, H. J. Senseless, a Zn finger transcription factor, is necessary and sufficient for sensory organ development in Drosophila. *Cell* **102**, 349–362 (2000).
36. Gerlitz, O. & Basler, K. Wingful, an extracellular feedback inhibitor of Wingless. *Genes Dev.* **16**, 1055–1059 (2002).
37. Giráldez, A. J., Copley, R. R. & Cohen, S. M. HSPG modification by the secreted enzyme notum shapes the Wingless morphogen gradient. *Dev. Cell* **2**, 667–676 (2002).
38. Kopke, D. L., Lima, S. C., Alexandre, C. & Broadie, K. Notum coordinates synapse development via extracellular regulation of Wingless trans-synaptic signaling. *Development* **144**, 3499–3510 (2017).
39. Port, F. & Bullock, S. L. Augmenting CRISPR applications in Drosophila with tRNA-flanked sgRNAs. *Nat. Methods* **13**, 852–854 (2016).
40. Couso, J. P., Bishop, S. A. & Martinez Arias, A. The Wingless signalling pathway and the patterning of the wing margin in Drosophila. *Development* **120**, 621–636 (1994).
41. Buchon, N. et al. Morphological and molecular characterization of adult midgut compartmentalization in Drosophila. *Cell Rep.* **3**, 1725–1738 (2013).
42. Tian, A., Benchabane, H., Wang, Z. & Ahmed, Y. Regulation of stem cell proliferation and cell fate specification by Wingless/Wnt signaling gradients enriched at adult intestinal compartment boundaries. *PLoS Genet.* **12**, e1005822 (2016).
43. Sato, A., Kojima, T., Ui-Tei, K., Miyata, Y. & Saigo, K. Dfrizzled-3, a new Drosophila Wnt receptor, acting as an attenuator of Wingless signaling in Wingless hypomorphic mutants. *Development* **126**, 4421–4430 (1999).
44. Sivasankaran, R., Calleja, M., Morata, G. & Basler, K. The Wingless target gene Dfz3 encodes a new member of the Drosophila Frizzled family. *Mech. Dev.* **91**, 427–431 (2000).
45. Gatti, M., Imhof, R., Huang, Q., Baudis, M. & Altmeyer, M. The ubiquitin ligase TRIP12 limits PARP1 trapping and constrains PARP inhibitor efficiency. *Cell Rep.* **32**, 107985 (2020).
46. Puppa, M. J. et al. Gut barrier dysfunction in the Apc(Min/+) mouse model of colon cancer cachexia. *Biochim. Biophys. Acta* **1812**, 1601–1606 (2011).
47. Cordero, J. B., Stefanatos, R. K., Myant, K., Vidal, M. & Sansom, O. J. Non-autonomous crosstalk between the Jak/Stat and Egfr pathways mediates Apc1-driven intestinal stem cell hyperplasia in the Drosophila adult midgut. *Development* **139**, 4524–4535 (2012).
48. Tian, A. et al. Intestinal stem cell overproliferation resulting from inactivation of the APC tumor suppressor requires the transcription cofactors earthbound and erect wing. *PLoS Genet.* **13**, e1006870 (2017).
49. Pai, L. M., Orsulic, S., Bejsovec, A. & Peifer, M. Negative regulation of Armadillo, a Wingless effector in Drosophila. *Development* **124**, 2255–2266 (1997).
50. Branon, T. C. et al. Efficient proximity labeling in living cells and organisms with TurboID. *Nat. Biotechnol.* **36**, 880–887 (2018).
51. Kajiro, M. et al. The E3 ubiquitin ligase activity of Trip12 is essential for mouse embryogenesis. *PLoS ONE* **6**, e25871 (2011).
52. Liu, X. et al. Trip12 is an E3 ubiquitin ligase for USP7/HAUSP involved in the DNA damage response. *FEBS Lett.* **590**, 4213–4222 (2016).
53. Keppler, B. R. & Archer, T. K. Ubiquitin-dependent and ubiquitin-independent control of subunit stoichiometry in the SWI/SNF complex. *J. Biol. Chem.* **285**, 35665–35674 (2010).

54. Griffin, C. T., Curtis, C. D., Davis, R. B., Muthukumar, V. & Magnuson, T. The chromatin-remodeling enzyme BRG1 modulates vascular Wnt signaling at two levels. *Proc. Natl. Acad. Sci. USA* **108**, 2282–2287 (2011).
55. Holik, A. Z. et al. Brg1 loss attenuates aberrant Wnt-signalling and prevents Wnt-dependent tumourigenesis in the murine small intestine. *PLoS Genet.* **10**, e1004453 (2014).
56. Collins, R. T. & Treisman, J. E. Osa-containing Brahma chromatin remodeling complexes are required for the repression of Wingless target genes. *Genes Dev.* **14**, 3140–3152 (2000).
57. Vasileiou, G. et al. Chromatin-remodeling-factor ARID1B represses Wnt/β-catenin signaling. *Am. J. Hum. Genet.* **97**, 445–456 (2015).
58. Dixon, A. S. et al. Nanoluc complementation reporter optimized for accurate measurement of protein interactions in cells. *ACS Chem. Biol.* **11**, 400–408 (2016).
59. Kaiho-Soma, A. et al. TRIP12 promotes small-molecule-induced degradation through K29/K48-branched ubiquitin chains. *Mol. Cell* **81**, 1411–1424.e1417 (2021).
60. Hanoun, N. et al. The E3 ubiquitin ligase thyroid hormone receptor-interacting protein 12 targets pancreas transcription Factor 1a for proteasomal degradation. *J. Biol. Chem.* **289**, 35593–35604 (2014).
61. Papoulas, O. et al. The HMG-domain protein BAP111 is important for the function of the BRM chromatin-remodeling complex in vivo. *Proc. Natl. Acad. Sci. USA* **98**, 5728–5733 (2001).
62. Weinstein, J. N. et al. The Cancer Genome Atlas Pan-Cancer analysis project. *Nat. Genet.* **45**, 1113–1120 (2013).
63. Tang, Z. et al. GEPIA: a web server for cancer and normal gene expression profiling and interactive analyses. *Nucleic Acids Res.* **45**, W98–W102 (2017).
64. Jones, S. et al. Core signaling pathways in human pancreatic cancers revealed by global genomic analyses. *Science* **321**, 1801–1806 (2008).
65. Radko-Juettner, S. et al. Targeting DCAF5 suppresses SMARCB1-mutant cancer by stabilizing SWI/SNF. *Nature* **628**, 442–449 (2024).
66. Liu, W. et al. RNF138 inhibits late inflammatory gene transcription through degradation of SMARCC1 of the SWI/SNF complex. *Cell Rep.* **42**, 112097 (2023).
67. Henderson, J. M. et al. Identification of HECT E3 ubiquitin ligase family genes involved in stem cell regulation and regeneration in planarians. *Dev. Biol.* **404**, 21–34 (2015).
68. Gudjonsson, T. et al. TRIP12 and UBR5 suppress spreading of chromatin ubiquitylation at damaged chromosomes. *Cell* **150**, 697–709 (2012).
69. Shanbhag, N. M., Rafalska-Metcalf, I. U., Balane-Bolivar, C., Janicki, S. M. & Greenberg, R. A. ATM-dependent chromatin changes silence transcription in cis to DNA double-strand breaks. *Cell* **141**, 970–981 (2010).
70. Chen, D., Yoon, J.-B. & Gu, W. Reactivating the ARF-p53 axis in AML cells by targeting ULF. *Cell Cycle* **9**, 3018–3023 (2010).
71. Belandia, B., Orford, R. L., Hurst, H. C. & Parker, M. G. Targeting of SWI/SNF chromatin remodelling complexes to estrogen-responsive genes. *EMBO J.* **21**, 4094–4103 (2002).
72. Link, K. A. et al. BAF57 governs androgen receptor action and androgen-dependent proliferation through SWI/SNF. *Mol. Cell Biol.* **25**, 2200–2215 (2005).
73. DiRenzo, J. et al. BRG-1 is recruited to estrogen-responsive promoters and cooperates with factors involved in histone acetylation. *Mol. Cell Biol.* **20**, 7541–7549 (2000).
74. Soderholm, S. & Cantu, C. The WNT/beta-catenin dependent transcription: a tissue-specific business. *WIREs Mech. Dis.* **13**, e1511 (2021).
75. Centore, R. C., Sandoval, G. J., Soares, L. M. M., Kadoch, C. & Chan, H. M. Mammalian SWI/SNF chromatin remodeling complexes: emerging mechanisms and therapeutic strategies. *Trends Genet.* **36**, 936–950 (2020).
76. Mittal, P. & Roberts, C. W. M. The SWI/SNF complex in cancer—biology, biomarkers and therapy. *Nat. Rev. Clin. Oncol.* **17**, 435–448 (2020).
77. Farnaby, W. et al. BAF complex vulnerabilities in cancer demonstrated via structure-based PROTAC design. *Nat. Chem. Biol.* **15**, 672–680 (2019).
78. Papillon, J. P. N. et al. Discovery of orally active inhibitors of Brahma Homolog (BRM)/SMARCA2 ATPase activity for the treatment of Brahma-related gene 1 (BRG1)/SMARCA4-mutant cancers. *J. Med. Chem.* **61**, 10155–10172 (2018).
79. Morin, X., Daneman, R., Zavortink, M. & Chia, W. A protein trap strategy to detect GFP-tagged proteins expressed from their endogenous loci in Drosophila. *Proc. Natl. Acad. Sci. USA* **98**, 15050–15055 (2001).
80. Tsuchiya, H. et al. Ub-ProT reveals global length and composition of protein ubiquitylation in cells. *Nat. Commun.* **9**, 524 (2018).
81. Hjerpe, R. et al. Efficient protection and isolation of ubiquitylated proteins using tandem ubiquitin-binding entities. *EMBO Rep.* **10**, 1250–1258 (2009).
82. Hughes, C. S. et al. Single-pot, solid-phase-enhanced sample preparation for proteomics experiments. *Nat. Protoc.* **14**, 68–85 (2019).
83. Valot, B., Langella, O., Nano, E. & Zivy, M. MassChroQ: a versatile tool for mass spectrometry quantification. *Proteomics* **11**, 3572–3577 (2011).
84. Schwanhäusser, B. et al. Global quantification of mammalian gene expression control. *Nature* **473**, 337–342 (2011).
85. Liao, Y., Wang, J., Jaehnig, E. J., Shi, Z. & Zhang, B. WebGestalt 2019: gene set analysis toolkit with revamped UIs and APIs. *Nucleic Acids Res.* **47**, W199–W205 (2019).
86. Savage, S. R., Shi, Z., Liao, Y. & Zhang, B. Graph algorithms for condensing and consolidating gene set analysis results. *Mol. Cell Proteom.* **18**, S141–S152 (2019).
87. Cerami, E. et al. The cBio cancer genomics portal: an open platform for exploring multidimensional cancer genomics data. *Cancer Discov.* **2**, 401–404 (2012).
88. Li, B. et al. Differential abundance of CK1α provides selectivity for pharmacological CK1α activators to target WNT-dependent tumors. *Sci. Signal* **10**, eaak9916 (2017).

Acknowledgments

We thank all members of the Lee and Ahmed laboratories for their insightful advice and discussion regarding this work and Ann Lavanway for her microscopy expertise. This work was supported by the National Institutes of Health (NIH) grants: T32GM008554 to S.K.; R35GM122516, and P50CA236733 to E.L.; R01CA219189 to D.J.R.; R01GM118557 to C.C.H.; R35GM136233, S10OD032310 to Y.A.; K08CA240901 and R01CA272875 to V.L.W.; R01GM118082 and R21HD101980 to R.R.; R35GM119455 to A.K.; T32GM007347 and F30CA281125 to M.A.L.; P30CA023108 to the Dartmouth Cancer Center; P20GM113132 to the Institute for Biomolecular Targeting; P40OD018537 to the Bloomington Drosophila Stock Center; U41HG000739 to FlyBase; and P40OD10949 to the Drosophila Genomics Resource Center. Support also came from the American Cancer Society grants 133934-CSDG-19-216-01-TBG and RSG-22-084-01-MM to V.L.W., the Intramural Research Program of the National Institutes of Health, National Cancer Institute Center for Cancer Research to A.M.L., and an Edwin H. Richard and Elizabeth Richard von Matsch Endowed Chair in Experimental Therapeutics and JPMorgan Private Bank to D.J.R.

Author contributions

S.K., A.C., M.R., A.S., L.G., G.O., and E.L. designed, performed, and analyzed the cultured cell and biochemical experiments. K.Y., N.B., B.M., A.A., M.M.A.A., Z.S., and Y.A. designed, performed, and analyzed the *Drosophila* experiments. N.B. and A.K. designed, performed, and analyzed the proteomics experiments. W.L. and D.J.R. designed, performed,

and analyzed the organoid experiments. L.R.N., C.W., and C.C.H. designed, performed, and analyzed the zebrafish experiments. M.A.L. and V.L.W. performed the multiplex immunofluorescence of colonic sections. G.X. and V.L.W. performed the TCGA analysis. AML and RR designed, performed, and analyzed the haploid genetic screens. D.R., A.D.M., X.W., F.Y., and O.K. provided intellectual guidance. E.L. and Y.A. provided intellectual guidance and reagents. S.K., K.Y., N.B., Y.A., and E.L. wrote the manuscript.

Competing interests

E.L. and D.J.R. are co-founders of StemSynergy Therapeutics, a company that seeks to develop inhibitors of major signaling pathways (including the Wnt pathway) for the treatment of cancer. The remaining authors declare that they have no competing interests.

Additional information

Supplementary information The online version contains supplementary material available at https://doi.org/10.1038/s41467-025-60535-5.

Correspondence and requests for materials should be addressed to Yashi Ahmed or Ethan Lee.

Peer review information *Nature Communications* thank Claudio Cantù, Jérôme Torrisani, and the other anonymous reviewer(s) for their contribution to the peer review of this work. A peer review file is available.

[1]Department of Cell and Developmental Biology, Vanderbilt University, Nashville, TN, USA. [2]Department of Molecular and Systems Biology, Geisel School of Medicine, Dartmouth College, Hanover, NH, USA. [3]Department of Biochemistry and Cell Biology, Geisel School of Medicine, Dartmouth College, Hanover, NH, USA. [4]Department of Medicine, Michigan State University College of Human Medicine, East Lansing, MI, USA. [5]Department of Oncology, Lombardi Comprehensive Cancer Center, Georgetown University, Washington, DC, USA. [6]Department of Pathology, Microbiology, and Immunology, Vanderbilt University Medical Center, Nashville, TN, USA. [7]Division of Biological and Biomedical Sciences, College of Health and Life Sciences, Hamad Bin Khalifa University, Doha, Qatar. [8]Department of Biostatistics, Vanderbilt University Medical Center, Nashville, TN, USA. [9]Laboratory of Cellular and Molecular Biology, Center for Cancer Research, National Cancer Institute, National Institutes of Health, Bethesda, MD, USA. [10]Department of Biochemistry, Stanford University School of Medicine, Stanford, CA, USA. [11]Dartmouth Cancer Center, Dartmouth College, Lebanon, NH, USA. [12]Vanderbilt Ingram Cancer Center, Vanderbilt University School of Medicine, Nashville, TN, USA. [13]These authors contributed equally: Sara Kassel, Kai Yuan. ✉e-mail: yashi.ahmed@dartmouth.edu; ethan.lee@vanderbilt.edu